Journal of Molecular Liquids 360 (2022) 119591

Contents lists available at ScienceDirect

Journal of Molecular Liquids

journal homepage: www.elsevier.com/locate/molliq

Interactions of polycyclic aromatic hydrocarbons and their nitro derivatives with bilayer and monolayer models of fungal membranes

Aneta Wójcik [a], Mareike Stephan [b], Weronika Ryczek [a], Karolina Olechowska [a], Paweł Wydro [c], Rumiana Dimova [b,*], Marcin Broniatowski [a,*]

[a] Department of Environmental Chemistry, Faculty of Chemistry, the Jagiellonian University in Kraków, Gronostajowa 2, 30-387 Kraków, Poland
[b] Max Planck Institute of Colloid and Interfaces, Science Park Golm, 14476 Potsdam, Germany
[c] Department of Physical Chemistry and Electrochemistry, Faculty of Chemistry, the Jagiellonian University in Kraków, Gronostajowa 2, 30-387 Kraków, Poland

ARTICLE INFO

Article history:
Received 22 April 2022
Revised 4 June 2022
Accepted 6 June 2022
Available online 9 June 2022

Keywords:
Fungal plasma membrane
Membrane modelling
Giant unilamellar vesicles
Langmuir monolayers
Polycyclic aromatic hydrocarbons (PAH)
Nitro-PAH
Persistent organic pollutants
Soil remediation
Grazing incidence X-ray diffraction
Brewster angle microscopy

ABSTRACT

Polycyclic aromatic hydrocarbons (PAH) are ubiquitous persistent organic pollutants forming as byproducts in combustion processes. These compounds can become nitrated in the environment forming even more toxic nitro derivatives. Both PAHs and nitro-PAHs accumulate in the soils which can lead to the pollution of vast areas of arable land. The best means of their elimination from the environment is bioremediation that is the degradation by soil microorganisms. Important key players with high prospects are non-ligninolytic fungi, which can incorporate PAHs and their derivatives into their plasma membranes, oxidize and metabolize to nontoxic products. The accumulation of PAHs in the membrane can, however, be toxic to the fungal cell, but the mechanisms of the PAH-membrane lipid interactions and how they influence the membrane phase state and properties are still poorly understood. To shed light on these questions we employed fungal plasma membrane models and studied their interactions with selected PAHs and nitro-PAHs. Two complementary model systems were investigated: giant unilamellar vesicles (GUV) and Langmuir monolayers. We find that the native PAHs induce phase separation and the formation of solid ordered phase in the GUVs, whereas the nitro-derivatives do not disturb the liquid crystalline state of the membranes. The Langmuir monolayer studies indicate that some PAHs preferably partition in the liquid-expanded phase while others in the liquid-condensed domains. The possibility of the incorporation of PAHs into the condensed domains implies that these compounds can influence the order in the lipid bilayer and affect the function of the lipid rafts in plasma membranes.

1. Introduction

Polycyclic aromatic hydrocarbons (PAH) are omnipresent organic molecules belonging to the class of persistent organic pollutants (POP) [1–3]. This classification is based on their toxicity, persistence in the environment and bioaccumulation in trophic chains. More than one hundred PAH congeners have been detected in environmental matrices. In the seventies of the previous century, the US Environmental Protection Agency (US EPA) specified 16 of them as reference environmental toxicants [4]. PAHs are dangerous to animals as their oxidized metabolites can be highly mutagenic and carcinogenic [5]. Indeed, benzo[a]pyrene (BAP) is one of the best known organic carcinogens [6], the concentration of which in the atmosphere is obligatory monitored in the European Union. PAHs are emitted in the atmosphere mainly from anthropogenic sources forming during the combustion of coal, fossil fuels and organic matter [7–9]. PAHs of lower molecular mass are present in the atmosphere mainly in gaseous phase, whereas higher molecular mass congeners are mainly adsorbed at soot particulate [10]. Contrary to unsubstituted PAHs, their oxidized derivatives are directly mutagenic and carcinogenic [11,12]. At high temperatures in the places of their generation, e.g. in engines, furnaces or waste incinerators, PAHs can react with nitrogen oxides forming nitro derivatives [13,14]. Furthermore, nitro-PAHs are formed by homogeneous or heterogenous reactions in the atmosphere of PAHs with hydroxyl radicals and nitrogen oxides during the days or with NO_3 radicals at night [15–17]. Although nitro-PAHs are present in much lower concentrations in the atmosphere they can be orders of magnitude more mutagenic and carcinogenic than the unsubstituted PAHs [18,19]. Both PAHs and their nitro derivatives can travel large distances from the emission sources before they are eliminated from the atmosphere by precip-

* Corresponding authors.
E-mail addresses: rumiana.dimova@mpikg.mpg.de (R. Dimova), broniato@chemia.uj.edu.pl (M. Broniatowski).

https://doi.org/10.1016/j.molliq.2022.119591
0167-7322/

itation or by dry deposition [20]. Due to their hydrophobicity PAHs and nitro-PAHs are practically water insoluble so they are targeted to soils and bottom sediments [21–23]. In soils, these compounds adsorb strongly on the surface of organic humic fractions or on soil minerals or frequently migrate into the porous soil particles and absorb therein [24]. The strong adsorption at and in the soil particular matter together with the hydrophobicity and aromaticity of the condensed rings contribute to the recalcitrance of these compounds in soils [21,24–26].

PAHs and their derivatives are not an easily accessible carbon source to soil microorganisms, so they accumulate in the soil, polluting large areas [27]. The accumulated PAHs can be mobilized by root exudates and assimilated by plants initiating their inclusion into the trophic chain [28]. Despite their limited accessibility, PAHs can be degraded by some species of soil bacteria and fungi. Multiple studies prove that in in-vitro conditions they can be the only carbon source for some decomposers [21,22,29–31]. If a large area of arable land is polluted by PAHs the only way of eliminating these pollutants is bioremediation [21]. The PAH biodegradation process can be augmented by biostimulation that is the provision of nutrients to the indigenous microorganisms, or by bioaugmentation, i.e. the inoculation of PAH degrading organisms into the soil [32]. Multiple bacterial and fungal species were reported to degrade PAHs [25,29–31]. In contrast to bacterial uptake of water soluble nutrients, hydrophobic substances are assimilated via release of biosurfactants and micellar solubilization [33]. The bacterial degradation of PAHs and their derivatives is hindered by the strong interaction of the compounds with hydrophobic humic particles or migration of the substances into the narrow pores of soil minerals that are not accessible for bacteria [24]. These limitations can be overcome by fungi.

In contrast to bacteria, fungal mycelia can grow in water unsaturated soil fractions by overgrowing aerial voids between the mineral particles or growing into the pores of the mineral grains [34,35]. Via chemotaxis the mycelia grow towards the potential carbon sources as well as to those connected with humic matter or absorbed inside the mineral particles [34]. The soil filamentous fungi are classified in ligninolytic and non-ligninolytic. The ligninolytic fungi, also termed white rod fungi, release ligninolytic enzymes such as lignin peroxidase, manganese-dependent peroxidase and laccase in their surrounding [36]. Since lignin and PAHs share high aromaticity, the ligninolytic enzymes can oxidize the adsorbed PAH molecules and, reduce their hydrophobicity. In this way, they induce their desorption and transform them into accessible carbon sources to the fungal cells. Multiple ligninolytic fungi were reported as effective PAH degraders [37–39]. Some non-ligninolytic fungi can also degrade PAHs and their derivatives. The mycelia of these fungi come in direct contact with the adsorbed PAH molecules and incorporate them into their plasma membranes, where these compounds are oxidized by cytochrome P450 and other monooxygenases [40,41]. Both ligninolytic and non-ligninolytic fungi can be inoculated into soils and applied for the remediation of polluted land. However, ligninolytic fungi depend on rotten wood as source of lignin. Therefore, their application in bioremediation requires addition of plant wastes as sawdust or straw [32,34]. Thus, non-ligninolytic fungi are more promising in the bioremediation of PAH contaminated soil due to their independence of lignin. These fungi accumulate the hydrophobic nutrients within their plasma membranes prior to their oxidation and further metabolism [34,42]. However, the accumulation of PAHs within the membrane can change its physical properties and in this way lead to fungal toxicity [43–45]. This problem is encountered especially for nitro-PAHs since nitroaromatics are frequently toxic to microorganisms [45,46]. The nitro group occurs very rarely in natural compounds; all known nitrocompounds synthesized by microorganisms are antibiotics [47]. Both, anabolic and catabolic pathways of nitro-aromatics are rare, leading to limited number of nitroaromatics-degrading bacteria and fungi. In vitro studies of fungal strains demonstrated that the accumulation of PAHs can change the membrane properties leading to the death of the cultivation [44,45,48]. However, the molecular mechanisms of the interactions of PAH molecules with the lipids of fungal membranes are still poorly understood. Moreover, the interactions of nitro-PAHs with membranes structural lipids have not been explored at all. One major question is whether PAH molecules and their mononitro-derivatives behave similarly or differently within the membrane environment. To answer this question and generally to shed light on the molecular mechanisms of the interactions of PAHs and their mononitro-derivatives with fungal membranes, we developed models of the fungal plasma membrane and studied their interactions with the pairs PAH/nitro-PAH. In our studies, three such pairs were investigated: pyrene/1-nitropyrene, fluoranthene/3-nitrofluoranthene and benzo[a]pyrene/6-nitrobenzo[a]pyrene. Pyrene and 1-nitropyrene are the main PAH and nitro-PAH products in car engine exhaust [49], nitrofluoranthene is the most abundant nitro-PAH in the atmosphere [50], whereas benzo[a]pyrene is the reference PAH carcinogen detected in multiple air-monitoring stations around the world [51]. Two complementary models of fungal membranes were employed: giant unilamellar vesicles (GUV) [52,53] and Langmuir monolayers.

2. Experimental

2.1. Materials

The lipids employed in our studies, 1,2-dimirystoyl-*sn*-glycero-3-phosphoethanolamine (DMPE), 1,2-dipalmitoyl-*sn*-glycero-3-phosphocholine (DPPC), 1-palmitoyl-2-oleoyl-*sn*-glycero-3-phosphocholine (POPC) and ergosterol, were purchased from Avanti Polar Lipids. The samples were lyophilized powders and were stored at −20 °C. The fluorescent probes Texas Red™ 1,2-dihexadecanoyl-*sn*-glycero-3-phosphoethanolamine triethylammonium salt (Texas-Red-DHPE) and, 1,1′-Dioctadecyl-3,3,3′,3′-Tetramethylindotri-carbocyanine Iodide ($DiIC_{18}$) were bought from Thermo Fischer. Pyrene (PYR), 1-nitropyrene (NPYR), fluoranthene (FLU), 3-nitrofluoranthene (NFLU), benzo[a]pyrene (BAP) and 6-nitrobenzo[a]pyrene (NBAP) all of the quality of analytical standards were purchased from Sigma Aldrich.

The structures of the studied pollutants are depicted in Scheme 1.

The solvents, HPLC grade chloroform (99.9%) stabilized by ethanol and HPLC grade methanol (99.9%) were bought from Sigma Aldrich. Sucrose (for molecular biology, ≥99.5%, HPLC grade), glucose (D-(+)-glucose), anhydrous, ≥99.5% (sum of enantiomers, HPLC grade) were purchased from BioUltra. Casein (from bovine milk, purified powder) was purchased from Sigma and polyvinyl alcohol (PVA fully hydrolyzed, Mw approx. 145000) was bought from Merck. Ultrapure water of resistivity of 18.2 MΩ·cm was produced in the laboratory from Merck Millipore water purification system.

2.2. Lipid solutions

Samples of the lipids were weighted on a Mettler Toledo balance with the accuracy of 10 μg and dissolved in chloroform/methanol 9/1 v/v mixture. The concentrations of the solutions applied for Langmuir monolayer formation were ca. 0.25 mg/mL (ca. $3.5 \cdot 10^{-4}$ M depending on the phospholipid and ca. $6.3 \cdot 10^{-4}$ M for ergosterol). PAHs and nitro-PAHs were also dissolved in chloroform/methanol 9/1 v/v mixture. If not indicated otherwise, the

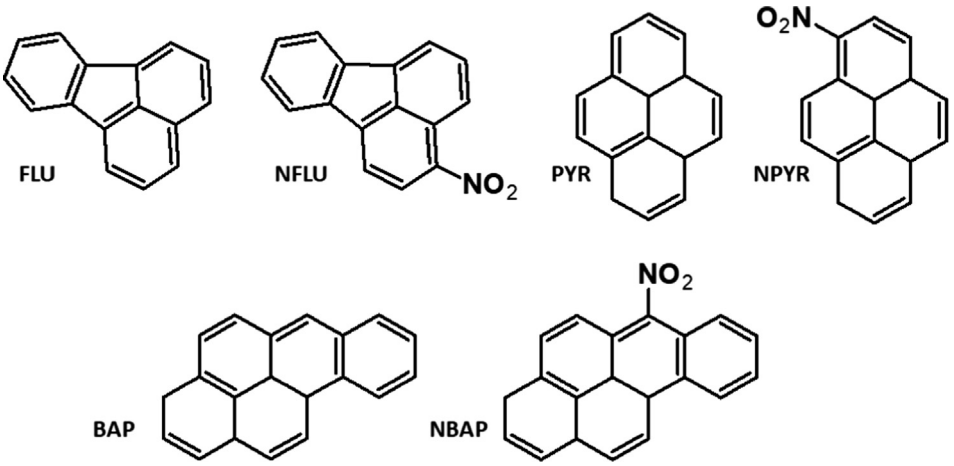

Scheme 1. Structural formulae of the studied PAHs and nitro-PAHs.

concentrations were 0.1 mg/mL, that is approx. $4{\cdot}10^{-4}$ M. The stock solutions were kept at −20 °C. The multicomponent lipid solutions were prepared in glass vials just before the experiments by mixing appropriate volumes of the stock solutions.

For GUV preparation, the following stock solutions were prepared (if not indicated otherwise the components were dissolved in chloroform): 10 mM POPC, 6 mM ergosterol, 10 mM PYR, 10 mM NPYR, 10 mM BAP, 4 mM NBAP and 8 mM DMPE (dissolved in chloroform/methanol 9/1 v/v mixture).

2.3. GUV preparation

The GUVs were prepared following the gel-assisted swelling method [54]. Briefly, sucrose and glucose solutions were prepared in Millipore water and filtered using a sterile membrane filter 0.45 μm (Whatman). The osmolality was measured with Osmomat 3000 (freezing point osmometer, Gonotec). 40 mg/ml PVA solution was prepared in MilliQ water and mixed in Thermomixer unit (750 rpm, 90 °C) for 40 min to obtain a homogeneous solution. The PVA solutions were stored at 35 °C for no longer than one week.

Microscope glass slides (cut edges, Roth, Karlsruhe) were first washed with ethanol, then rinsed plentifully with Millipore water and dried under nitrogen stream. 50 μl of PVA solution was spread on the cleaned glass and kept for 30 to 40 min at 50 °C to allow PVA drying. Then, on the still hot glass 5 μl of 4 mM lipid solution containing 0.5 mol% of Texas Red-DHPE was spread and dried under vacuum for 30 min. A swelling chamber was built using a rectangular Teflon spacer sandwiched between two lipid-coated glass slides. The chamber was filled with 2 ml of 100 mM sucrose solution and immediately placed in an oven (Thermo Scientific, Heraeus vacutherm) at 55 °C. After 15 min the GUVs were harvested and transferred into a tube. The sample was slowly cooled down to room temperature on an aluminum block at a cooling rate of approximately 1 °C/min. The sample was used within 12 h.

2.4. GUV imaging

Coverslips (22 × 40 mm) were coated for 40 min with 10 μl 2 mg/ml casein aqueous solution before being rinsed with water and dried under a nitrogen stream. The observation chamber was formed by a spacer and two coverslips. For the sample preparation, 50 μl of GUVs solution was mixed with 90 mM glucose solution. 70 μl samples were placed in the observation chamber and kept for 40 min in the dark to allow the GUVs to settle down. The observations were performed on a Leica TCS SP8 microscope. Cross section images were acquired using a HC PL FLUOTAR L 40x/ NA 0.60 dry objective, while the z-stacks were obtained using a HCP APO CS 63x/ NA 1.2 water-immersion objective. The GUVs containing $DiIC_{18}$ as the fluorescent probe were excited with DPSS 561 nm laser line at 5% intensity and 10% gain of the detector (HyD) in the wavelength range 570 nm – 610 nm. GUVs containing Texas Red-DHPE as the fluorescent probe were excited with the same laser line at 2% intensity and 10% gain, and the emission was collected in the same range.

GUVs containing benzo[a]pyrene without the fluorescent probes were excited with a diode 405 nm laser line with 100% intensity and 100% gain and the emission signal collected between 570 nm and 610 nm. Images (512 × 512 pixels) were recorded in the bidirectional scan mode at 400 Hz. A z-stack scan was carried out of half of the GUV (upper or lower part) to avoid overlapping projections. The images were analyzed with the Leica software (LAS X).

2.5. Differential scanning calorimetry - DSC

Multilamellar vesicles (MLV) were prepared from the same stock solutions as GUVs by the hydration of dry lipid film in glass vials to the final concentration of 1 mM. The measurements were performed with VP-DSC MicroCal calorimeter equipped with a calorimetric cell (Tantalum, 0.5 ml). Using an analytical syringe, 0.5 ml of the MLV sample was introduced in the cell, while the reference cell was filled with degassed MilliQ water. The DMPE MLVs were studied at the temperature ranging from 25 to 70 °C, whereas the other samples were studied between 10 and 60 °C. The samples were heated/cooled at the rate of 1 °C/min. For each sample two heating and one cooling scans were applied. All experiments were repeated at least twice for different MLV samples.

2.6. Langmuir monolayer technique

Three Langmuir troughs were employed in the studies: a double barrier KSV-NIMA (Biolin Scientific, Sweden) trough of total area of 273 cm^2 was used for the routine π-A isotherm registration, a larger double barrier KSV-NIMA trough of total area of 580 cm^2 was used in the BAM experiments, whereas in the SOLEIL Synchrotron at the Sirius beamline a custom R&K single barrier trough of an approximate area of 500 cm^2 was installed. After an experiment, the monolayer material was disposed from the surface with a vacuum aspirator and then the subphase was removed. The troughs were wiped first with a tissue soaked in chloroform then with isopropanol and rinsed with plentiful of ultrapure water. MilliQ ultra-

pure water was applied as the subphase in all experiments performed on Langmuir troughs. The troughs were filled with MilliQ water and the appropriate volume of lipid chloroform solution were deposited at the water/air interface with the application of Hamilton analytical syringes. The troughs were left for 10 min for chloroform evaporation, then the monolayers were compressed at compression rate of 10 mm·min^{-1}. The surface pressure π was monitored with a Wilhelmy-plate electrobalance (KSV NIMA) with a rectangular plate of filtration paper (Whatman, ashless) applied as surface pressure sensor with the uncertainty of ± 0.05 mN/m. The π-A isotherms were measured at least three times and the uncertainty of the mean molecular area A was ± 1 Å/molecule. The temperature of the subphase was controlled by a water-circulating bath. All the experiments were performed at 20 ± 0.1 °C.

The compression modulus C_S^{-1} was calculated from the course of the π-A isotherms according to its definition [55]: $C_S^{-1} = -A\frac{\partial\pi}{\partial A}$.

2.7. Brewster angle microscopy

UltraBAM instrument (Accurion GmbH, Goettingen, Germany) equipped with a 50 mW laser emitting p-polarized light at a wavelength of 658 nm, a 10 × magnification objective, polarizer, analyzer and a CCD camera was used. The spatial resolution of the microscope was 2 μm. The foregoing apparatus and the Langmuir trough were placed on a table (Standa Ltd., Vilnius, Lithuania) equipped with active vibration isolation system (antivibration system VarioBasic 40, Halcyonics, Göttingen, Germany).

2.8. Grazing incidence X-ray diffraction

The experiments were performed at the SIRIUS beamline in SOLEIL synchrotron (Gif-sur-Yvette, France) using the dedicated liquid surface diffractometer [56]. The Langmuir trough (R&K GmBh electronics, Germany) was mounted on the goniometer in a gas tight box with Kapton windows. The applied energy of the X-ray beam (7.92 keV, λ = 1.565 Å) is high which can result in serious beam damage to the investigated monolayer. To avoid these phenomena, the experimental chamber was sealed and carefully flashed with helium to reduce the oxygen level to values lower than 1%, as most of the beam damages are related to the generation of reactive oxygen species and the oxidation of the phospholipid molecules. Then the monolayer was compressed to the target surface pressure of 20 mN/m (see explanation below), which afterward was held constant during the entire experiment. The detailed construction of the diffractometer working at the SIRIUS beamline and the parameters of the synchrotron beam applied in the GIXD experiments are described on the SOLEIL web site (https://www.synchrotron-soleil.fr). The scattered signal was detected using a Pilatus3 2D pixel detector (Dectris Ltd., Switzerland). This detector is used as 1D detector through the combined use of a Soller slits collimator oriented vertically to fix the in-plane 2θ resolution and an integration of the 2D image horizontally to obtain a 1D spectrum. The achieved resolution was about 0.002 Å^{-1}. The spectra were obtained by scanning the in–plane 2θ angle. At each point, the vertically scattered intensity was recorded to obtain finally the intensity map $I(Q_{xy},Q_z)$, where Q_{xy} is the scattering vector component in the monolayer plane, and Q_z is the vertical component along the z-axis. The $I(Q_{xy},Q_z)$ diffractograms were integrated along the vertical distribution of Q_z to obtain the Bragg peaks $I(Q_{xy})$. The estimation of the full width at half maximum (FWHM) of Bragg peak enables the calculation of the L_{xy} parameter, which is related to the range of 2D crystallinity, $L_{xy} \approx 0.88 \cdot 2\pi/\mathrm{FWHM}_{peak}$. Further details of this technique can be found in the introductory papers by Kjaer [57] and Als Nielsen et al. [58]. All the GIXD experiments were performed on monolayers compressed to 20 mN/m. This is a value lower than 30 mN/m usually accepted as the pressure at which the packing of acyl chains in the monolayer is comparable to that in the bilayer. However, both at 20 and at 30 mN/m the π-A isotherm of membranes of mixture M2 (defined later in the text) were very steep, with approximately the same slope, and the corresponding C_S^{-1} values in both cases suggest liquid condensed state of the monolayer. Also BAM images depicted practically identical morphology of the M2 monolayer both at 20 and at 30 mN/m. For the GIXD experiment the monolayer is compressed to the required surface pressure and kept in that conditions for about one hour. Therefore, we avoided the pressure of 30 mN/m as at that condition 3D lipid aggregates frequently evolve from the Langmuir monolayers, which then slowly collapse with time.

3. Results and discussion

3.1. Construction of the fungal membrane models

The composition of plasma membrane of yeast and filamentous fungi as reported in multiple studies, resembles that of other eukaryotic plasma membranes, namely containing phosphatidylcholines PC, phosphatidylethanolamines PE, phosphatidylserines PS, phosphatidylinositols PI, ergosterol and sphingolipids [59,60]. In contrast to bacteria, fungal membranes do not usually contain phosphatidylglycerols PG, and cardiolipins are found predominantly in mitochondrial membranes. Early work exploring the mutual proportion of phospholipids in yeast plasma membrane, underlined the role of PS as the dominating phospholipid [61]. This observation was, however, not corroborated by later articles. Generally, the two dominating phospholipid classes are PC and PE, at comparable fractions [59,62]. In a typical fungal membrane PC and PE constitute 80% of all phospholipids while PS and PI constitute the remaining 20% [59,62,63]. This generalization regards both yeast and filamentous fungi. In some species, PC dominates over PE (molar ratio of 6/4) [62] and some strains with PC constituting 80 % of the phospholipid pool have been also observed [64]. The lipid acyl chains of the membrane phospholipids are either both unsaturated, or saturated in the sn1 chain and unsaturated in the sn2 chain [65,66]. The acyl chain in the sn1 position has the average length of 16 carbon atoms, whereas the average length of the acyl chain in the sn2 position is 17, as palmitoleic (16C) and oleic (18C) acid rests are most frequently found in this position [65]. Therefore, 1-palmitoyl-2-oleoyl-*sn*-glycero-3-phospholipids are considered suitable components of fungal plasma membrane models [67,68]. Ergosterol is the most widespread fungal lipid and its role for the membrane structure and function is crucial [69]. In the yeast lipidome, ergosterol constitutes about 10 mol % of all lipids [60]; however, its fraction in the membrane can vary considerably depending on the membrane type. Moreover, ergosterol is the main component of lipid rafts in fungal membranes so its distribution within the membrane is not uniform. In earlier studies, there have been claims that the ergosterol/phospholipid ratio in the fungal plasma membrane can be even 3; however, others argue that the value of 1 is much more realistic [70]. The ergosterol distribution is not only uneven but can be changed by the fungus depending on the development stage, environmental conditions or the presence of antibiotics or toxins [71]. Therefore, in most studies on model fungal membranes the ergosterol/phospholipid ratio ranges from 0.1 to 1 [72].

Our model was based on POPC, as phosphatidylcholines are the main phospholipid class of the fungal plasma membrane, and the sn1-palmitoyl-sn2-oleoyl substitution of the glycerol backbone mimics the average distribution of acyl chains in these phospholipids [70]. As the second component of our model we selected

DMPE, as phosphatidylethanolamines are typically the second most widely distributed phospholipid class within the fungal membranes. PEs have often more saturated acyl chains [73]; therefore, we chose DMPE as a suitable representative. On the other hand, DMPE being completely saturated has a relatively low main transition temperature T_m of 48 °C [74], which is convenient for liposome preparation. The molar proportion of POPC to DMPE was varied between 6/4 and 4/6 mimicking variations in PC/PE ratio in many yeast and filamentous fungi [70,75]. The third component of our model was ergosterol (ergo), the mole ratio of which was established experimentally, see Fig. 1, using the following criteria. Generally, a functional plasma membrane should be liquid crystalline, so in the code of model lipid bilayers in liquid disordered, L_d or liquid ordered, L_o phase, while solid ordered S_o (gel) phase should be avoided. We examined vesicles at different fraction of ergosterol to locate the optimal composition.

A sharp transition at T_m = 48 °C was observed for DMPE in accordance with literature [74]. For the POPC/DMPE 6/4 mol/mol mixture a wide transition at ca. 30 °C was observed (Fig. 1b), whereas for the ternary system containing additionally 10 mol% of ergosterol, a wide shallow transition could still be observed in the DSC scan (Fig. 1c). Increasing the ergosterol content to 15 mol% eliminated any transition peaks (Fig. 1d). We employed the fluorescent probes: $DiIC_{18}$ and Texas Red-DHPE which preferentially partition in the liquid L_o or L_d phases and are excluded from the solid domains leaving them to appear dark in microscopy images. For the POPC/DMPE 6/4 mixture, the S_o phase occupies a large area of the vesicle (see Fig. 1e), which is in accordance with the DSC data presented in Fig. 1b. Indeed, the wide DSC peak ranging from ca. 18 to 35 °C suggest phase separation in the studied system. The introduction of ergosterol at X(erg) = 10 mol% reduces the area occupied by the S_o phase in the GUV image but still both liquid and solid phases coexist in the vesicles (Fig. 1 f). At and above X(ergo) = 15 mol% the GUVs appeared uniformly red and homogenous, no phase separation was observed (Fig. 1g,h), which is in accordance with the lack of any DSC peaks for this composition (Fig. 1d).

To ensure a liquid crystalline state of the bilayer and to mimic fungal plasma membrane composition, we selected the ternary system POPC/DMPE/erg 51/34/15 in mol%. We will refer to this mixture as M1. The Langmuir monolayer studies employed a second model mixture, M2 in which POPC was replaced by DPPC, namely DPPC/DMPE/erg 51/34/15 mol%. The main transition temperature (T_m) for DPPC is 43 °C higher than for POPC (41 *vs* −2 °C, respectively), which significantly increases the chain ordering within the monolayers. This is of crucial importance for the effective employment of the GIXD technique and can be of help in the BAM visualization of the studied systems.

3.2. Studies of the incorporation of PAHs and nPAHs to GUVs

The effects of two pairs of PAHs/nitro-PAHs, namely PYR/NPYR and BAP/NBAP, on the physical properties of the lipid bilayers in the GUV model (of composition M1) of fungal membranes were studied, whereas in the part devoted to Langmuir monolayers a third pair FLU/NFLU was additionally investigated. Fluoranthene is an isomer of pyrene, thus, the employment of the additional pair PAH/nitro-PAH enabled the more in-depth discussion of the correlation between the PAH structure and its interaction with model membranes.

Considering the aromatic structure of the compounds (containing multiple benzene rings), we questioned whether their presence

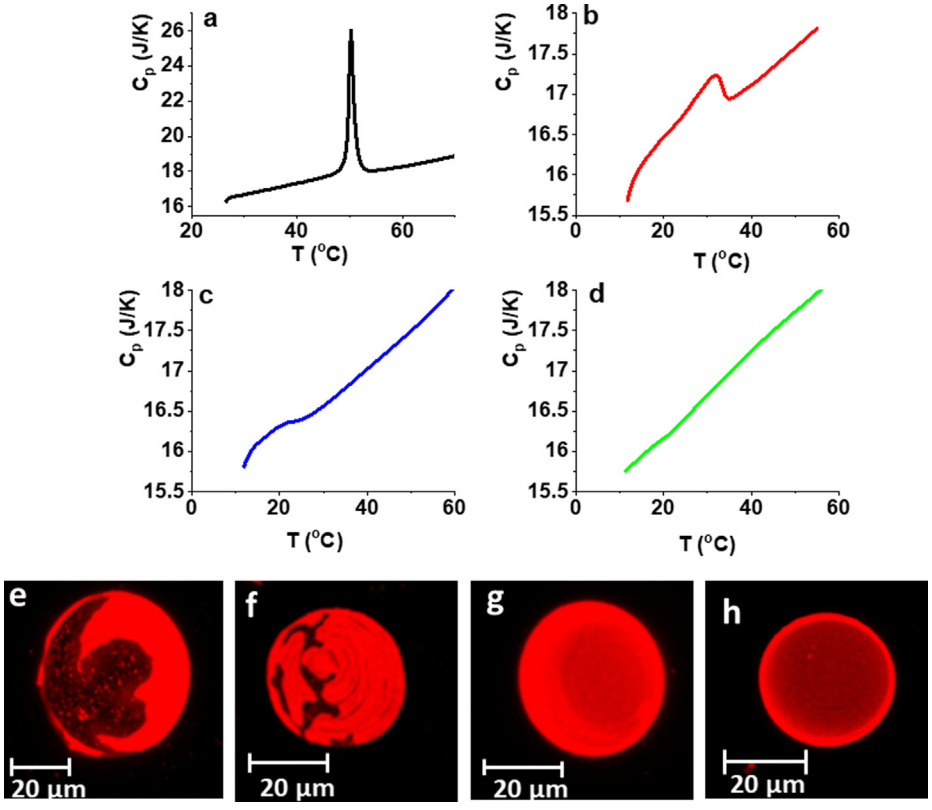

Fig. 1. a-d) DSC plots for: a) pure DMPE, b) POPC/DMPE 6/4 mol/mol mixture, c) POPC/DMPE/ergo with POPC/DMPE 6/4 and X(ergo) = 10 mol %, d) POPC/DMPE/ergo with POPC/DMPE 6/4 and X(ergo) = 15 mol%, e-h) confocal images of the upper half of GUVs formed from: POPC/DMPE 6/4 mol/mol and various fractions of ergosterol: e) X (ergo) = 0, f) X(ergo) = 10 mol%, g) X(ergo) = 15 mol%, h) X(ergo) = 20 mol%. The GUV membrane was doped with 0.5 mol% of the fluorescent probe $DiIC_{18}$ and was observed at 20 °C.

and incorporation in the GUV membrane can be imaged microscopically. Indeed, the pyrene moiety is frequently grafted to fluorescent probes [75,76]. The quantum yield of BAP is even higher than that of PYR [77], whereas the substitution of the nitro group to one of the rings severely extinguishes the fluorescence signal [78]. Therefore, BAP was selected for the further experiments. GUVs of three different compositions were formed: (1) model M1 composition (Fig. 2a), (2) model M1 composition doped with 10 mol% BAP (Fig. 2 b) and (3) model M1 composition doped with 10 mol% BAP and 0.5 mol% $DiIC_{18}$ (Fig. 2c).

GUVs of the model M1 composition lacking BAP and $DiIC_{18}$ are not fluorescent (Fig. 2a). The fluorescence signal emitted by GUVs doped with 10 mol% BAP corroborates its presence in the lipid bilayer (Fig. 2b), but the relatively low signal as generated by our microscopy system suggests that high-quality imaging is not feasible. On the other hand, the fluorescence observed for the GUV containing also the membrane dye $DiIC_{18}$ excited at 561 nm (Fig. 2c) shows that simultaneous imaging of $DiIC_{18}$ and BAP in the same GUV is feasible. However, continuous imaging of BAP and quantitative analysis was avoided because of the required strong laser intensity (see Methods), which could lead to artifacts from potential photodamage. In Fig. 2c, we also see that the $DiIC_{18}$ signal is no longer homogeneous as in the case of the BAP-free membrane (compare to Fig. 1g) suggesting phase separation induced by the PAH molecules. Thus, in the following, we explored the membrane phase state upon addition of BAP, NBAP, PYR and NPYR at 10 and 20 mol%. The resultant images are presented in Fig. 3.

GUVs of model M1 POPC/DMPE/ergo 51/34/15 labeled with Texas-Red-DHPE show homogeneous liquid crystalline phase (Fig. 3a) as already shown for vesicles labeled with $DiIC_{18}$ (Fig. 1g). In this part of the experiments $DiIC_{18}$ was exchanged by Texas Red-DHPE, as in the model systems doped by the investigated PAHs and nitro-PAHs, especially at 20 mol% of these pollutants, $DiIC_{18}$ was observed to form aggregates appearing as puncta of high intensity. This artefact was not observed for Texas Red-DHPE; thus, $DiIC_{18}$ was replaced by Texas Red-DHPE. The

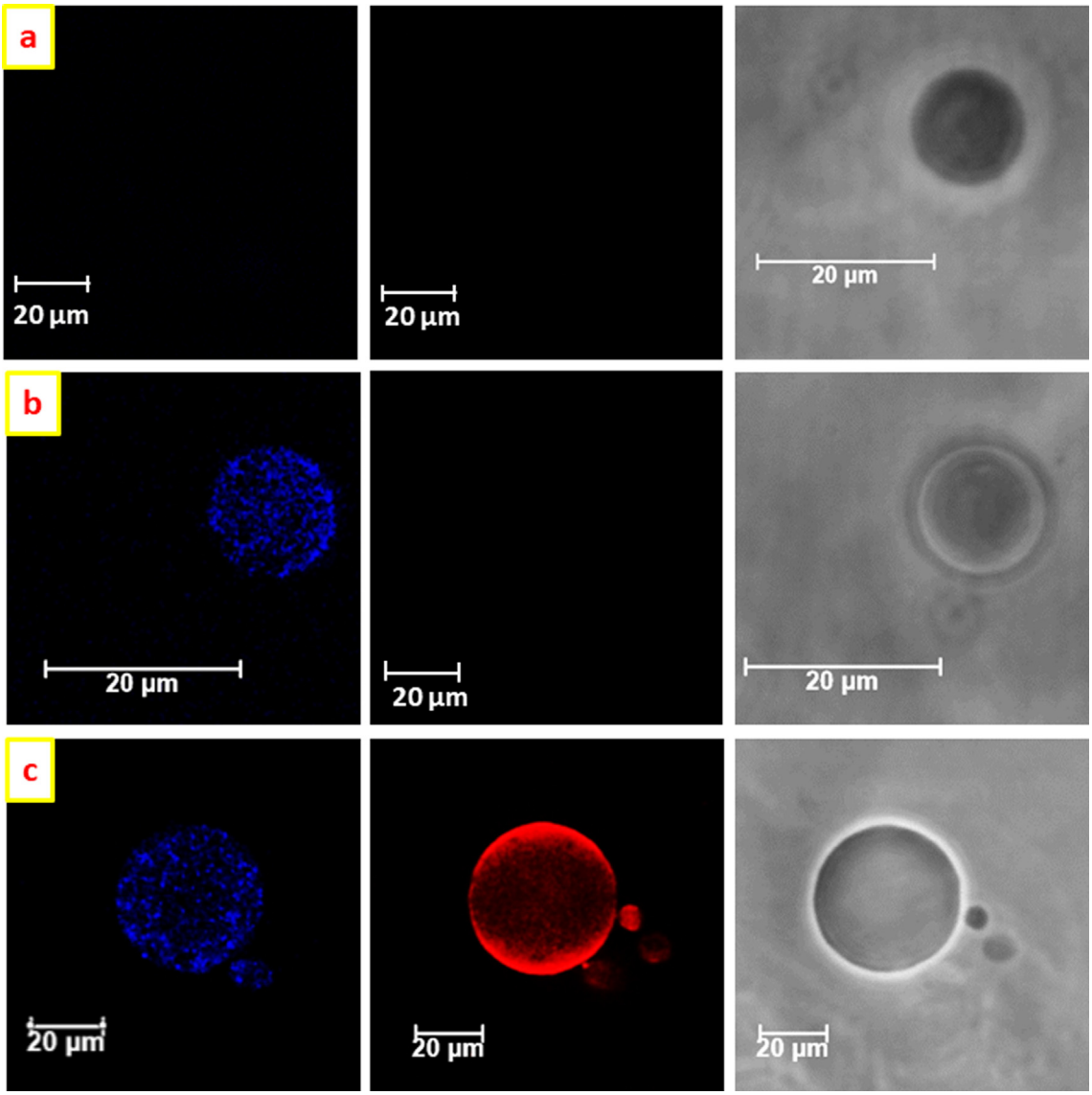

Fig. 2. Confocal and phase contrast images of GUVs with three different compositions to probe the reconstitution and detection of PAH in the membrane: a) POPC/DMPE/ergo 51/34/15, no addition of fluorescent probe and PAHs, b) POPC/DMPE/ergo 51/34/15 with 10 mol% BAP (blue channel), c) POPC/DMPE/ergo 51/34/15 with 10 mol% of BAP and 0.5 mol% $DiIC_{18}$ (red channel). The images in the first column show BAP signal upon excitation at 405 nm and emission signal collected in the range 413 nm – 469 nm, in the second column the membrane signal from $DiIC_{18}$ excited at 561 nm and emission signal collected in the range 570 nm – 610 nm; last column shows phase contrast images. (For interpretation of the references to colour in this figure legend, the reader is referred to the web version of this article.)

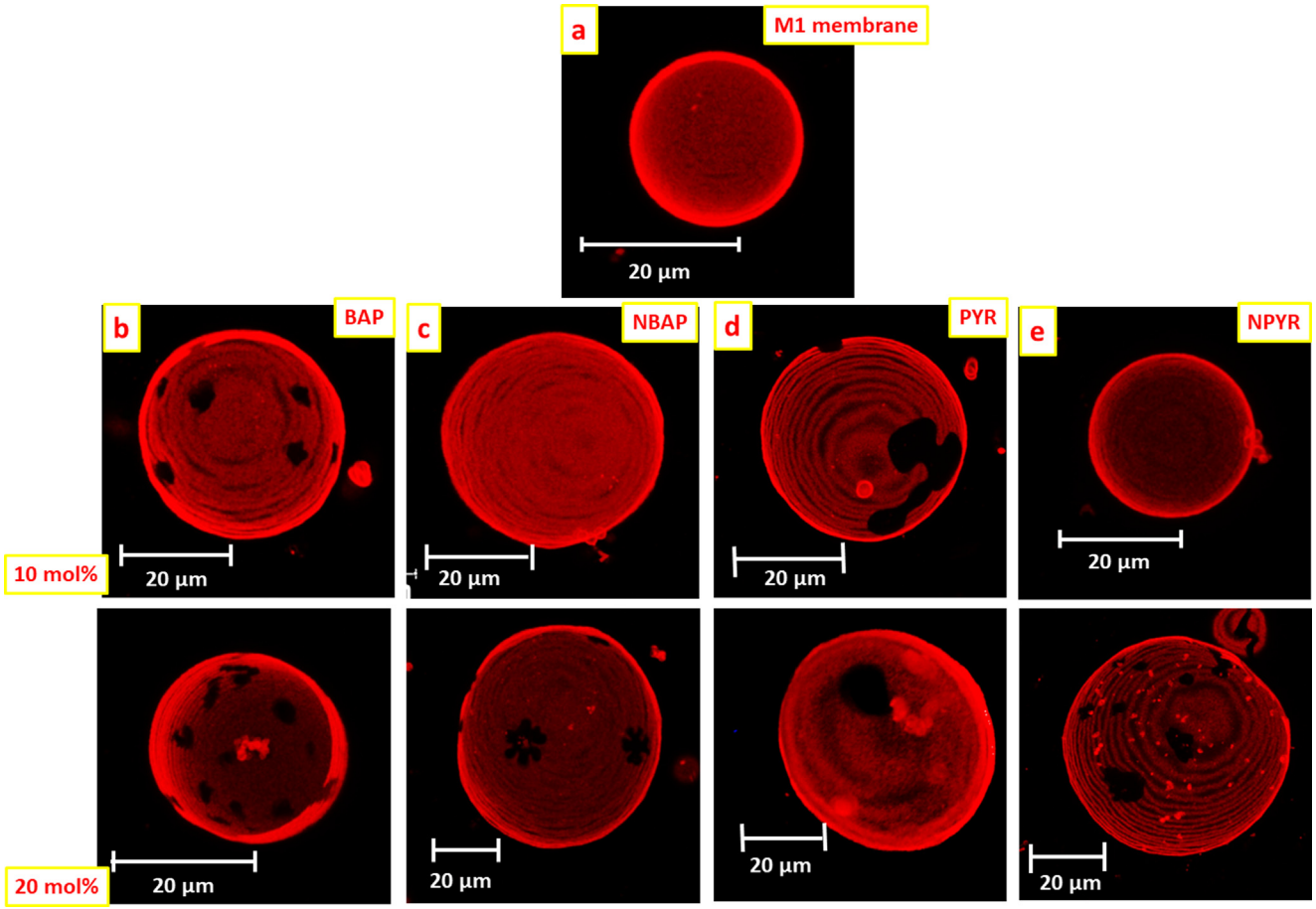

Fig. 3. Maximum projection images of representative confocal 3D series of the upper half of vesicles composed of mixture M1 and containing the investigated PAHs and 0.5 mol% of Texas Red-DHPE. The GUVs contained either 10 mol% or 20 mol% of the investigated PAHs/nitro-PAHs as indicated in the images. (For interpretation of the references to colour in this figure legend, the reader is referred to the web version of this article.)

addition of 10 mol% of BAP to the ternary lipid mixture induces considerable changes in the membrane phase state (Fig. 3b). Dark domains appear in the GUV membrane. The domain shape is irregular and preserved over time suggesting S_o phase, thus, indicating an increase in the order of the acyl chains induced by BAP resulting in phase separation. This phenomenon is even more pronounced in the presence of PYR (Fig. 3d), as the S_o domains occupy even larger area of the vesicle surface. Interestingly, the incorporation of the mononitro derivatives NBAP and NPYR does not cause phase separation. The increase of the mole fraction of the pollutants to 20% results in the formation of solid domains in all GUVs. Moreover, in some GUVs, as for example at X(NPYR) = 20%, bright spots can be observed, suggesting potential aggregation of the fluorescent probe by the increased concentration of the pollutant (as was the case of $DiIC_{18}$ at even lower concentration). Upon examination of the phase contrast images of the vesicles, we observe that, upon incorporation of both PAH and their nitro derivatives, the contrast of the vesicles is preserved: vesicles remain dark due to the asymmetry of sucrose/glucose solutions across the membrane and the difference in their refractive indices, see last column of Fig. 2b,c. This implies that the membranes are not leaky in the presence of PAH and nitro-PAH, or at least not permeable to molecules of size comparable to and larger than that of sucrose and glucose.

Overall, our results on the bilayer GUV model of the fungal plasma membrane prove that the native PAHs as BAP or PYR condense the bilayer inducing phase separation and formation of gel S_o phase. If such phenomena occurred *in vivo*, this might lead to cell death due to drastic change of the membrane fluidity and associated permeability change. At low concentration (10 mol%), the more polar PAH nitro derivatives do not cause phase separation in the model membranes. This could be a result of either lesser condensing effect on the bilayer or potential lower incorporation in the bilayer, which we are not able to resolve in the GUV model. The observed phase separation at the higher concentration (20 mol %) is an interesting and valuable observation and illustrates the situation of hypothetical overloading of the membrane with the incorporated PAHs and nitro-PAHs.

3.3. Studies of the monolayer models

Further studies were performed on a different membrane model, that is Langmuir monolayer. Although Langmuir monolayers are one-molecule-thick, mimicking only one leaflet of the plasma membrane they are versatile platforms for membrane modeling [79], as multiple factors can be controlled that are inaccessible in vesicle studies. Moreover, multiple microscopic, spectroscopic and X-ray diffraction techniques can be effectively applied for the monolayers' characterization. Two models of fungal plasma membrane were applied in the studies of Langmuir monolayers – M1 (POPC/POPE/ergo 51/34/15, as in the case of GUV studies) and M2 in which POPC was exchanged for DPPC. The monolayers were compressed and the surface pressure (π) – mean molecular area (A) isotherms were recorded. The results for M1 model monolayers doped with the investigated PAHs and nitro-PAHs at various fractions are presented in Fig. 4.

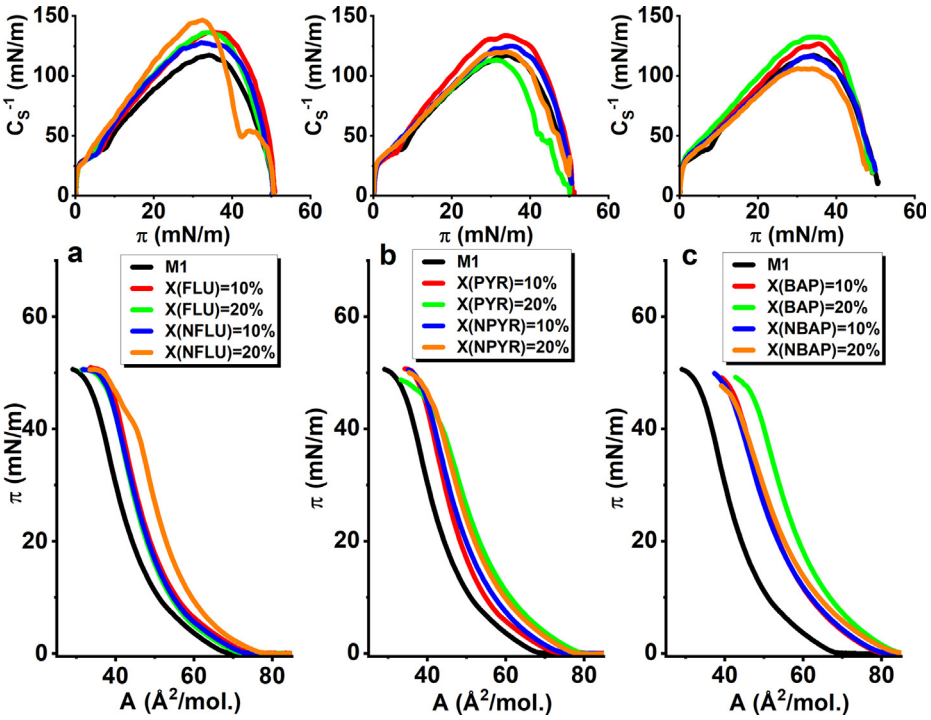

Fig. 4. π-A isotherms and C_S^{-1}-π dependences registered for the M1 monolayers doped with various fractions of: a) FLU and NFLU, b) PYR and NPYR, c) BAP and NBAP. The molar fractions of the introduced PAH and nitro-PAH are given in the legends.

It should be underlined that all the applied PAHs and their mononitro derivatives are not surface active. Therefore, the number of the polar lipid molecules at the air water interface was kept constant in all the experiments. To achieve the declared mole ratios X of the pollutants the total number of the molecules (lipids + pollutants) deposited at the interface was increased. In such an approach the incorporation of the POP molecule in the monolayer leads to the shift of the π-A isotherm toward larger mean molecular area. All the applied PAHs and nitro-PAHs are not soluble in water and have limited volatility, causing them to stay at the air/water interface when deposited there. If the molecules are not able to incorporate in the monolayer, they form 3D aggregates or adsorptive layers (so called add-layers [80]) on top of the polar lipid monolayers. In such a case the location of the π-A isotherm at the X-axis and the course of the isotherm are unchanged and identical with the curve registered for the monolayer without the POP addition.

The addition of all the investigated PAHs and nitro-PAHs to the M1 monolayer leads to the shift of the isotherms toward larger mean molecular areas. For the isomeric PAHs PYR and FLU the isotherm shift is practically identical, namely ca. 4 Å^2/mol. at 20 mN/m, whereas for BAP larger shifts – ca. 11 Å^2/mol. at 20 mN/m were observed. All the π-A isotherms for the monolayers doped by the investigated pollutants remained shifted toward larger mean molecular area till the monolayers collapse. This implies that the incorporated POP molecules were not squeezed out from the lipid monolayer at high surface pressure values. At X(POP) = 10%, the π-A isotherms for the M1 monolayers doped by the nitro derivatives overlap with the isotherms of the parent PAH molecules, so the substitution of one nitro group does not change the packing pattern of the studied pollutants within the matrix of the lipid hydrophobic moieties in the M1 monolayer. The mole ratio of 20% was more differentiating for the investigated POP. We observed that for FLU the π-A isotherm registered at X(FLU) = 20% overlapped with that registered at X(FLU) = 10%. This means that the incorporation of this molecule in the M1 monolayer was limited and that the increase of the number of FLU molecules deposited at the air/water interface did not increase the number of the molecules built into the monolayer.

This cannot be said about the nitro derivative NFLU, as the isotherm registered at X(NFLU) = 20% is 5 Å^2/mol. shifted (at 20 mN/m) toward larger mean molecular areas than the curve measured at X(NFLU) = 10%. Thus, it can be stated that the introduction of the nitro group increases the limits of the number of the POP molecules which can be incorporated in the model fungal membrane. Regarding the π-A isotherm measured for the M1 monolayer containing 20 % of NPYR it should be also underlined that at a high pression of ca. 40 mN/m a deflection point is clearly visible in the course of the isotherm. This is probably connected with the elimination of the excess NPYR molecules from the monolayer in that conditions.

For PYR the π-A isotherm registered at X(PYR) = 20% is 6 Å^2/mol. (at 20 mN/m) shifted toward larger mean molecular areas than the curve registered at X(PYR) = 10%, which proves that significantly more PYR than the FLU molecules can be accumulated in the model membrane. At both studied mole fractions the isotherms for the monolayers doped by PYR overlap with the curves measured for the membranes enriched in NPYR. It can be inferred from these results that the possibility of the incorporation of the PAH molecules into the polar lipid Langmuir monolayer and the number of such molecules which can be built therein is strictly related to the structure of the PAH molecules. Some PAH isomers get incorporated whereas others not, or at much lower quantities, which is in accordance with the conclusions drawn by us in the previous studies performed for different membrane models and on different PAH congeners [81]. From all pollutants investigated here, BAP was most easily incorporated in the M1 model membrane. The high affinity of this particular PAH to lipid monolayers was corroborated by previous studies [81,82]. However, an interesting outcome is that the π-A isotherms registered for the M1 monolayer doped by NBAP at X(NBAP) = 10% and 20% overlap, and the isotherm registered at X(NBAP) = 20% is 4 Å^2/mol. shifted toward smaller mean

molecular areas than the curve registered at X(BAP) = 20%. This means that the conclusion regarding the incorporation of nitro-PAHs inferred from the data collected for the pair FLU/NFLU is not so straightforward. The case of the BAP/NBAP pair proves that for some PAHs the introduction of the nitro group can lower the limit of the number of the molecules which can be built into the lipid membrane. In such a case the nitro group is probably a steric hindrance disturbing the interactions of the PAH molecules with the hydrophobic moieties of the membrane lipids.

Compression moduli C_S^{-1} were calculated from the course of the π-A isotherms and in the form of the C_S^{-1}-π plots are also presented in Fig. 4. The maximal value of C_S^{-1} observed for the M1 monolayer is 116 mN/m, which as a value higher than 100 mN/m implies that at higher surface pressures this monolayer achieves the liquid condensed (LC) state [55]. However, when studied with Brewster angle microscopy, this monolayer remained completely homogeneous in the BAM images suggesting that it was in the liquid expanded (LE) state till its collapse. The formation of condensed domains within this monolayer would be analogous to the formation of S_o phase in the GUVs, so the lack of such domains is in accordance with the data discussed in the section devoted to the characterization of M1 GUVs. The addition of PYR and BAP to the monolayer increases the C_S^{-1} values proving the conclusions regarding the condensing effect drawn from the GUV studies. However, in the case of the monolayers no phase separation or condensed domains formation was observed for the M1 monolayer doped by these PAHs, suggesting a plausible role of leaflet coupling, monolayer curvature and its possible asymmetry in the GUV bilayer system. The nitro derivatives NPYR and NBAP had no effect on the course of the C_S^{-1}-π curve as the curves registered for monolayers doped by these pollutants overlapped with the curve measured for the pure M1 monolayer. This observation is again in accordance with the studies performed on GUVs as at the presence of NPYR and NBAP at X = 10% the vesicles remained homogeneous and no S_o domains were observed. Only for the M1 monolayer doped by NFLU the C_S^{-1} values were noticeably higher than for the undoped membrane, but in this case the presence of the nitro group generally mitigated the incorporation of this PAH into the membrane, changing its elasticity. The deflection point discussed for the π-A isotherm measured for the monolayer at X(NFLU) = 20% results in a local minimum in the course of the C_S^{-1}-π curve.

Reacting to external stress as increased concentration of ethanol, toxicants or antibiotics, fungi frequently modify the composition of their plasma membrane. This is achieved by changing the mutual proportions of the main polar lipids forming the monolayer as well as by the change of the saturation of the acyl chains [73,83]. Therefore, in our studies we introduced a second model M2 of the fungal plasma membrane in which the mixed chain POPC was exchanged for saturated chain DPPC. Identical experiments discussed above were also performed for this model and the resultant π-A isotherms and C_S^{-1}-π plots are presented in Fig. 5.

The π-A isotherm registered for the M2 model has different course than the curve discussed above for the M1 model monolayer. The characteristic feature of this curve is a plateau region observed for mean molecular areas ranging from 60 to 47 Å^2/mol. and surface pressure values from 4 to 6 mN/m. Similar plateau can be observed in the π-A isotherm registered for pure one-component DPPC monolayer [84] and it should be reminded that DPPC is the main component of the M2 model constituting 51% of its components. Such a plateau in the course of the π-A isotherm is the manifestation of the LE-LC transition in the investigated monolayer [79]. The compression modulus C_S^{-1} calculated from the course of this isotherm reaches the value of 100 mN/m at π = 20 mN/m and the maximal value of 240 mN/m at π = 40 mN/m. The course of the isotherm and the C_S^{-1} values prove that at the surface pressure of ca. 5 mN/m LC domains appear in the monolayer and that at higher surface pressure most lipid molecules in this monolayer are involved in LC domain formation. Similarly to the M1 model, doping of the monolayer with the investigated PAHs and nitro PAHs leads to a shift of the isotherms proving the incorporation of these molecules into the model membrane. However, the observed sequences of the isotherm and their shifts from the curve registered for the pure M2 monolayer are significantly different than these described for the M1 model. This observation proves that the saturation of the acyl chains is a crucial factor affecting the incorporation of hydrophobic molecules into the membrane. For the M1 model the effects of BAP incorporation were most pronounced. For the M2 model, the largest shifts of the isotherms are observed for FLU and especially NFLU. This further corroborates the conclusion that the introduction of the nitro group in the 3 position of fluoranthene increases its membrane activity. At the high surface pressures – 30 and more mN/m till the monolayer collapses, the isotherms registered at X (FLU) = 10% and 20% practically overlap with the curve measured for the pure M2 model. This could imply that at higher surface pressures FLU molecules are eliminated from the monolayer. However the collapse pressures at X(FLU) = 10 and 20 % were noticeably higher than for the undoped M2 model which means that at least some FLU molecules remained incorporated into the model membrane increasing its condensation. The same cannot be said about the M2 monolayer doped by NFLU since even at high surface pressure values the isotherms do not overlap with the curve measured for M2 and at 30 mN/m the isotherm measured at X(NFLU) = 20% is 10 Å^2/mol. shifted toward larger mean molecular areas. For PYR and NPYR the isotherms measured at X = 10% and 20% overlap with each other, but all are shifted toward larger areas compared to the curve measured for POP-free M2. This means that at lower surface pressure values limited amounts of PYR and NPYR can be incorporated into the model membranes. BAP exhibit increased affinity to lipid layers [81,82], therefore it was effectively incorporated in the M2 model membrane, since at surface pressures close to the collapse pressure the isotherm registered at X(BAP) = 20% was still ca. 6 Å^2/mol. shifted toward larger mean molecular areas. As it was already observed for the M1 model the substitution of one nitro group to the 6 position of benzo[a]pyrene profoundly decreases the incorporation of this PAH into the model membrane, since the π-A isotherms registered for NBAP were similar to these measured for NPYR.

Since the M2 monolayer was much less compressible than the M1 model, the incorporation of PAHs and nitro-PAHs had a negligible impact on the course of the C_S^{-1}-π curves. The two most diverging curves were registered at X(FLU) = 20% and X (NPYR) = 20%. In both cases, the maximum value of C_S^{-1} significantly decreased from 240 mN/m to 160 mN/m and 140 mN/m, respectively. This observation is probably connected with the formation of multiple 3D aggregates formed by FLU and NPYR after their expulsion from the monolayer. Such aggregates incrusting the monolayer can severely affect its elasticity resulting in different courses of the C_S^{-1}-π curves.

The application of the saturated-acyl-chain phospholipids for the formation of the M2 model fungal membrane enabled the effective application of Brewster angle microscopy for the visualization of the M2 monolayer, pure and doped by the investigated pollutants. The representative images taken at π = 20 mN/m are shown in Fig. 6.

As discussed above, a plateau ranging from 4 to 6 mN/m and 60 to 47 Å^2/mol. is present in the course of the π-A isotherm of the M2 monolayer. At that condition LC domains form in the monolayer upon its compression. At 20 mN/m the domains are well developed and dominate the BAM image. These domains are roughly circular, with a serrated edge and the average diameter of 20 μm. The addition of 10 mol% of FLU leads to the decrease of the average diam-

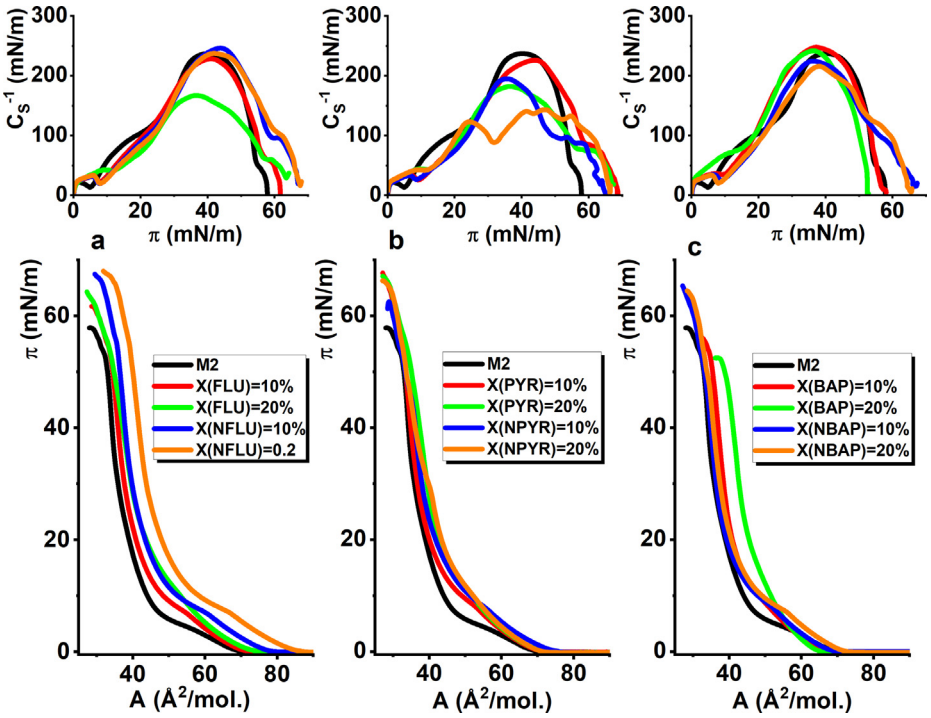

Fig. 5. π-A isotherms and C_S^{-1}-π dependences registered for the M2 monolayers doped by POPs at different fractions as indicated in the legend: a) FLU and NFLU, b) PYR and NPYR, c) BAP and NBAP.

eter of the condensed domains to ca. 5 μm and to the significant increase of their number. The darker regions of the monolayer in the LE state still visible in Fig. 6a are significantly reduced, but the small LC domains do not coalesce completely to form a homogeneous film. The increase of X(FLU) to 20% leads to the formation of multiple 3D aggregates of FLU molecules which were not incorporated into the monolayer. This phenomenon is in accordance with the characteristics of the π-A isotherms measured at X (FLU) = 10% and 20%, as both the curves overlapped proving that the excess FLU molecules were not built into the lipid film. The addition of NFLU also lowers the average diameter of the LC domains to ca. 10 μm. These domains are visibly larger and less numerous than it was observed for FLU. It should be underlined that some tiny 2D aggregates can be observed in the photo (Fig. 6e), which can be connected with the successive elimination of some NPYR molecules at higher surface pressures. At X (NFLU) = 20% the 3D aggregates were visible in the BAM images but they were significantly less numerous than for FLU, which corroborates the conclusion drawn from the isotherm analysis, that the introduction of the nitro group to the FLU molecule facilitates its incorporation into the lipid membrane. Doping the M2 model membrane with PYR leads to the further decrease of the diameters of the LC domains. Now the diameters are in the resolution limit of the microscope that is below 2 μm, so some interference fringes can be observed in Fig. 6c illustrating this monolayer. The increase of X(PYR) to 20% leads to the formation of multiple tiny 3D aggregates formed by the excess PYR molecules which cannot build into the model membrane. The M2 monolayers doped by NPYR, BAP and NBAP at X = 10% at 20 mN/m were practically homogeneous, which proves the condensing effect of these molecules exerted on these membranes. The mole proportion of 20% of these pollutants exceeds the limits of the number of the molecules which can be effectively included into the lipid matrix, so multiple 3D aggregates were observed.

The formation of the M2 model membrane of saturated lipids: DPPC, DMPE and ergosterol, which are all known to form 2D crystalline periodically ordered Langmuir monolayers [85] enabled the application of the Grazing incidence X-ray Diffraction technique for the further characterization of the M2 monolayer. This technique provides the direct information about the packing of the film-forming molecules within the monolayer plane with Ångstrom resolution, that is about the type of the 2D crystal lattice, the lattice parameters, the collective tilt of the acyl chains from the monolayer normal and about the range of 2D crystallinity. All the three lipids forming the M2 model membrane form separately 2D crystalline films, but this does not guarantee the periodical packing of the acyl chains in their ternary mixture Therefore, the first question was whether the M2 monolayer was 2D crystalline. It turned out, that a strong diffraction signal was registered for this monolayer compressed to 20 mN/m and the resultant GIXD data are presented in Fig. 7.

Two distinct separate diffraction signals are present in the GIXD intensity map. One of them centered at Q_{xy} = 1.48 Å^{-1} has its intensity maximum at horizon, that is at Q_z = 0 Å^{-1}. The second signal centered at Q_{xy} = 1.42 Å^{-1} has its itensity maximum at Q_z = 0.48 Å^{-1}. The intensity of the signal at Q_{xy} = 1.42 Å^{-1} is approximately two times greater than that of the signal at Q_{xy} = 1.48 Å^{-1}. Such a location of the diffraction signals in the reciprocal space as well as the ratio of their intensities are determinant for the rectangular centered 2D lattice with the hydrocarbon chains tilted towards the nearest neighbor (the NN azimuth) [57,58], so the signals were identified with the Miller indices h,k, as < 0,2 > and < -1,1>, respectively. The lattice parameters a, b and γ, the area of the unit cell A, tilt angle τ and the range of crystallinity L_{xy} were calculated from these data and are gathered in Table. 1.

GIXD experiments were also performed for the M2 monolayers doped by the investigated PAHs and nitroPAHs at the mole ratio of these pollutants of 10%. No experiments were performed at X = 20%, as the nucleation of multiple 3D aggregates in these monolayers excludes the application of this technique. The results obtained for these monolayers are presented in the form of Bragg peak pro-

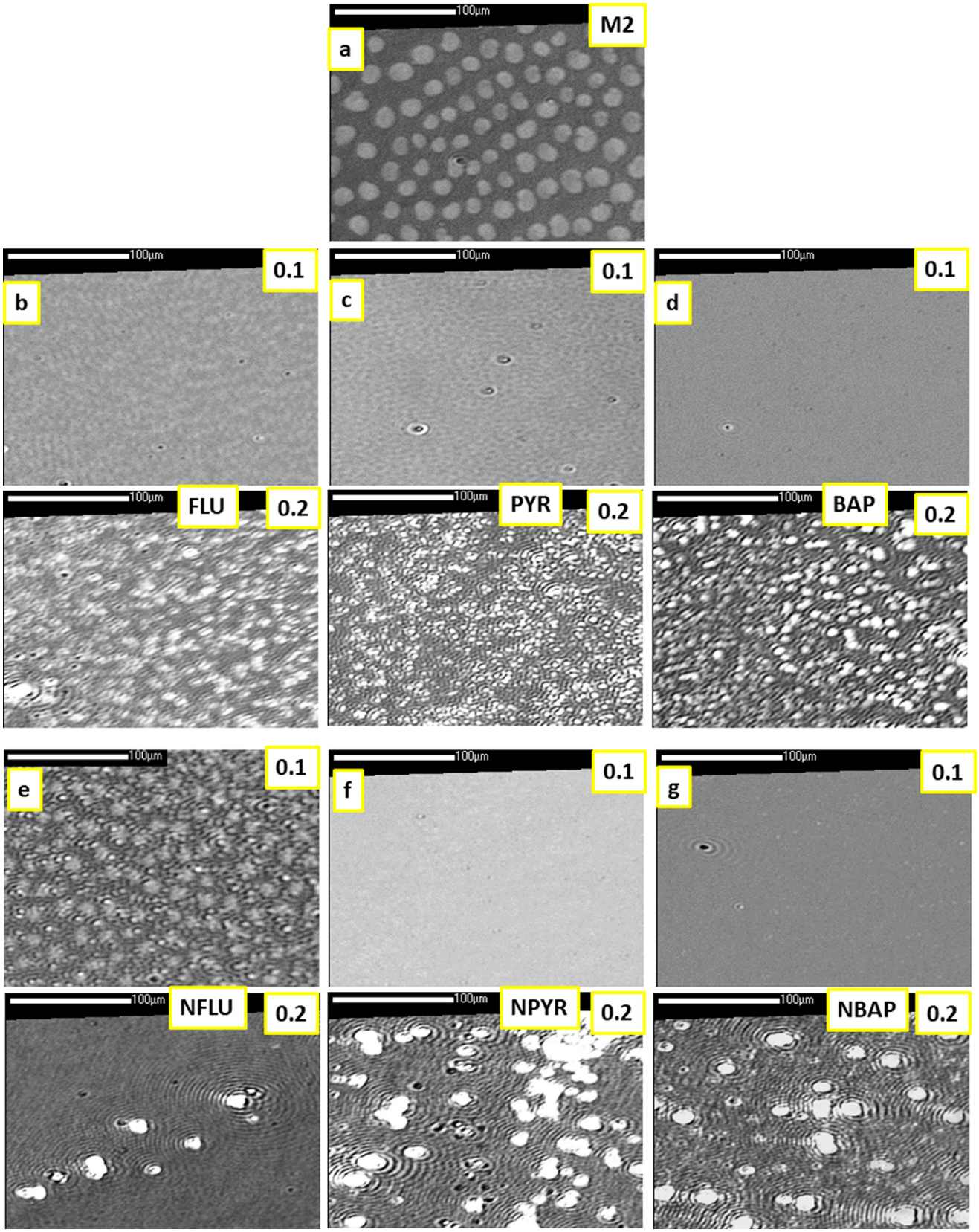

Fig. 6. Representative BAM images taken at 20 mN/m upon the compression of the monolayers of the M2 model. a) pure M2 monolayer, b-g) M2 monolayer with the addition of the investigated PAHs and nitro-PAHs at X = 10% and 20%. The scale bars denote 100 µm.

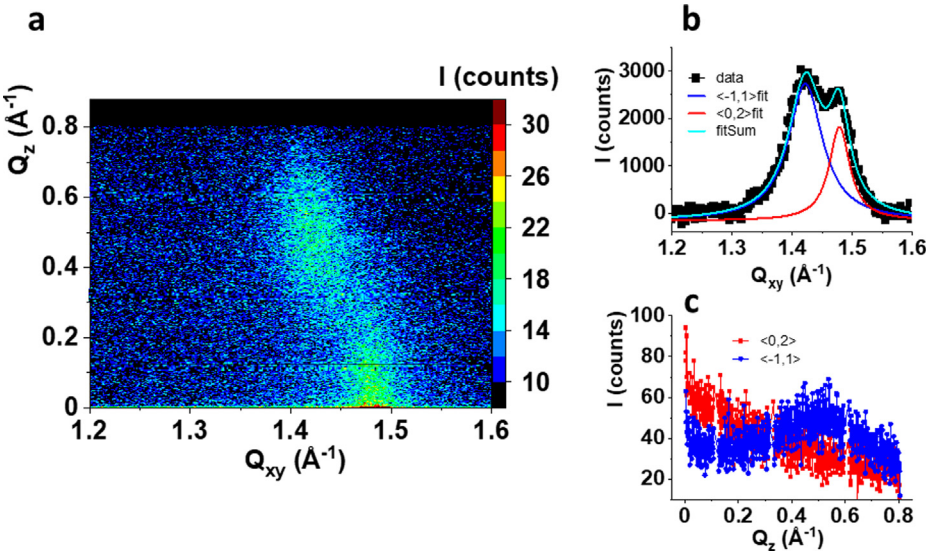

Fig. 7. GIXD results for the M2 model membrane. a) I(Q_{xy},Q_z) intensity map, b) Bragg peak profiles, I(Q_{xy}) and c) Bragg rod profiles, I(Q_z). Solid lines in panel b are best fits of the Lorentz curves to the experimental data.

Table 1
Structural parameters calculated from the results of GIXD experiments performed for the pure M2 membrane and for the membrane doped by the investigated PAHs and nitroPAHs at X = 10%.

system	2D lattice	a, b, γ (Å, Å, deg)	A (Å^2)	τ (deg)	L_{xy} (Å)
M2	Rectangular centered	5.173, 8.497, 90	43.95	21.8	$_{<-1,1>}$ 79 ± 1 $_{<0,2>}$ 132 ± 6
X(FLU) = 10%	Rectangular centered	5.202, 8.479, 90	44.11	23.0	$_{<-1,1>}$ 79 ± 1 $_{<0,2>}$ 135 ± 5
X(NFLU) = 10%	Rectangular centered	5.184, 8.451, 90	43.81	22.0	$_{<-1,1>}$ 59 ± 3 $_{<0,2>}$ 108 ± 5
X(PYR) = 10%	oblique	4.956, 5.012, 117.47	22.04	21.6	$_{<0,1>}$ 75 ± 2 $_{<1,0>}$ 50 ± 2
X(NPYR) = 10%	Rectangular centered	5.180, 8.468, 90	43.86	19.5	$_{<-1,1>}$ 80 ± 5 $_{<-1,1>}$ 92 ± 3 $_{<0,2>}$ 395 ± 28
X(BAP) = 10%	oblique	4.874, 5.030, 117.63	21.73	19.5	$_{<0,1>}$ 79 ± 4 $_{<1,0>}$ 58 ± 3
X(NBAP) = 10%	oblique	4.915, 5.016, 117.17	21.93	19.4	$_{<-1,1>}$ 64 ± 5 $_{<0,1>}$ 74 ± 6 $_{<1,0>}$ 129 ± 10 $_{<-1,1>}$ 129 ± 7

files in Fig. 8, whereas all the structural parameters calculated from these data are gathered in Table. 1.

The analysis of the GIXD results obtained for the M2 monolayer enriched in the investigated PAHs and nitro-PAHs leads to the conclusion that the presence of FLU and NFLU in the monolayer practically does not affect its 2D structure. The Bragg peak profiles (Fig. 8 a and b) for these monolayers were practically identical with the profile for the pure M2 monolayer presented in Fig. 7b, so also all the structural parameters for the three monolayers presented in Table 1 are comparable. This is an interesting result as FLU and NFLU were recognized to be the molecules more easily incorporating into the M2 monolayer as compared with the other four compounds investigated here. The explanation of this apparent contradiction can be found in the BAM images. The addition of FLU and NFLU to the M2 monolayer leads to the noticeable reduction of the diameter of the LC domains but the darker homogenous regions in the images being the manifestation of the LE phase are still present and their total area is comparable with that observed for the pure M2 monolayer. Thus, it can be inferred from that data that the FLU and NFLU molecules are located in the LE phase of the model membrane and are not included into the LC domains. Only the LC domains can be periodically ordered and diffract the X-rays, so the lack of any noticeable changes in the GIXD data for M2 monolayer enriched in FLU and NFLU means that these molecules are not incorporated into these domains. The addition of PYR to the M2 monolayer do not lead to a noticeable change of the molecular tilt or the lattice parameters, but to the change in the azimuth of the tilt which was changed from NN to the intermediate direction [86]. This reorientation of the acyl chains resulted in the change of the type of the 2D crystalline lattice from rectangular centered observed for M2 to oblique in the presence of PYR. The L_{xy} parameter describing the range of 2D crystallinity is anisotropic both in the rectangular centered and oblique lattice, so its values should be discussed with the indication of the crystallographic direction. For M2 the L_{xy} value in the < 0,1 > direction is 132 Å, whereas the largest value of this parameter in the < -1,1 > direction in the monolayer enriched in PYR was 80 Å, so it can be stated that the incorporation of this pollutant to the LC domains decreases the range of their 2D crystallinity. For the monolayer enriched in NPYR the crystal lattice was rectangular centered as in the case of pure M2 monolayer. The structural parameters are also similar, however, a discernable decrease of the tilt angle can be observed for the monolayer doped in NPYR. Interestingly, the L_{xy} value in the < 0,2 > direction is 395 Å, that is 3 times greater than observed

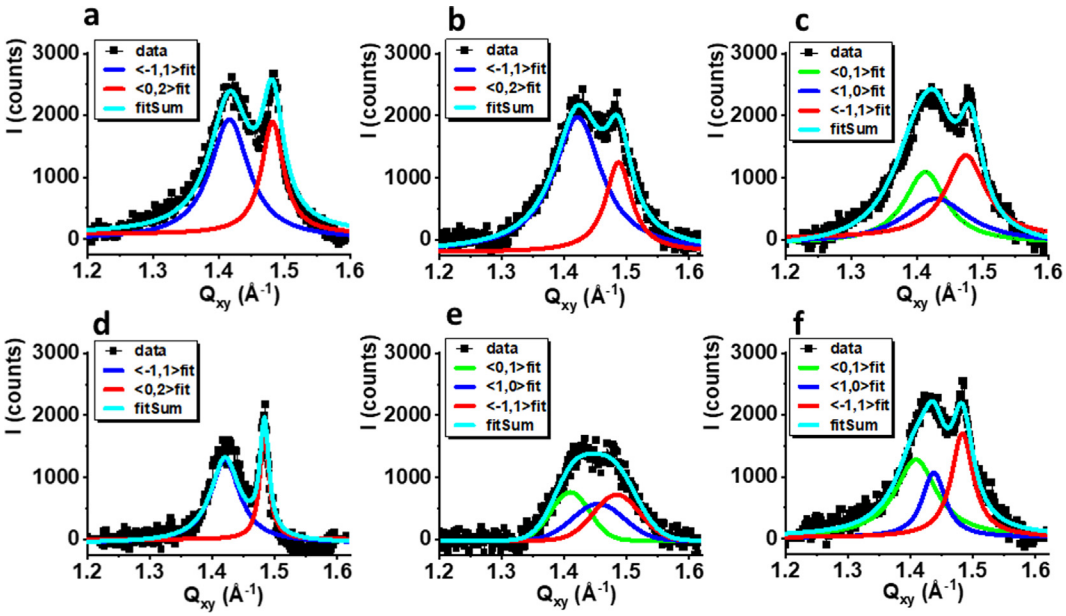

Fig. 8. Bragg peak profiles I(Q_{xy}) measured for the M2 monolayer doped with 10% of the following pollutants: a) FLU, b) NFLU, c) PYR, d)NPYR, e) BAP, f) NBAP. Solid lines are best fits of the Lorentz curves to the experimental data.

for the pure M2 monolayer. Thus, NPYR when incorporated to the LC domains increases significantly the range of 2D crystallinity. BAP and NBAP when incorporated to the M2 monolayer change the azimuth of the molecular tilt from NN to the intermediate resulting in the change of the 2D lattice from rectangular centered observed for the M2 monolayer to the oblique observed for M2 enriched in these substances. NPYR, BAP and NBAP are compounds which profoundly change the morphology of the M2 model membrane in the mesoscale, which was documented by the BAM images. The large separated LC domains observed for pure M2 model membrane merge in the presence of these pollutants leading to the homogenization of the monolayer. The GIXD results proved that all the three substances can build into the condensed domains, but they differ considerably regarding their effects on the range of 2D crystallinity. NPYR exerts an organizing effect on these domains – the manifestation of this are the narrow Bragg peak profiles observed in the reciprocal space and the threefold increase of L_{xy} observed in the real space. On the contrary, BAP disorganizes the ordering of the crystalline domains – the Bragg peaks are wider, and in consequence the range of crystallinity, expressed in the value of the L_{xy} parameter, diminishes. Finally, NBAP practically does not affect the range of 2D crystallinity when built into the crystalline domains.

The main conclusions from this part of the studies can be summarized as follows. The ability of a PAH molecule to incorporate in the more organized and condensed domains in the membrane depends on the structure of a given PAH. Certain PAHs such as FLU and NFLU prefer more expanded membrane regions and do not incorporate in condensed domains. Other PAHs and nitro-PAHs are included into such domains, whereby they change the ordering patterns of the acyl chain of the domain-forming lipids. It should be underlined that the fungal plasma membrane is not a pool of uniformly distributed lipids but multiple lipid rafts or generally more condensed domains can form in it [70]. The formation of these domains depends on the development stage of the fungal cell and its metabolic needs. Typically, such domains are enriched in ergosterol, sphingolipids and membrane proteins. When included into such domains, PAHs and nitro-PAHs can disturb their structure or perturb the function of enzymatic proteins included therein, disturbing the metabolism of the fungal cell.

4. Summary and conclusions

Our studies were devoted to the interactions of polycyclic aromatic hydrocarbons and their mononitro derivatives with models of fungal plasma membrane. PAHs and nitro-PAHs accumulate in the soils which can lead to the contamination of vast areas of arable land [21,24,87]. The perspective means of remediation of PAH polluted soils is bioremediation based on the application of PAH degrading non-ligninolytic soil fungi [40,41,88,89]. These fungi accumulate the molecules of highly hydrophobic pollutants in their plasma membranes where these compounds are oxidized, which enables their further metabolism [87]. However, the accumulation of PAHs and nitro-PAH can induce toxic effects resulting from the perturbations of the membrane structure caused by these substances [43,45]. In our studies we applied two complementary membrane models: giant unilamellar vesicles and Langmuir monolayers. The interactions of PAHs both with the lipid bilayers as well as with monolayers depend significantly on the structure of a given PAH molecule as well as on the presence of the nitro substituent. Using fluorescence microscopy, we proved that benzo[a]pyrene effectively incorporate into the lipid bilayer of the GUVs mimicking the fungal membrane. The incorporation of the native PAHs at the level of 10 mol% in the vesicle bilayer induced phase separation and the formation of S_o domains. This phenomenon could have negative consequences occurring in real membranes, as the active plasma membrane of a living cell should be in the liquid crystalline fluid state [90]. The formation of large solid domains is expected to drastically affect the membrane functionality with lethal consequences for the microorganisms [91]. On the other hand, nitro derivatives when incorporated into the membrane do not induce the S_o phase formation as the GUVs remained fluid and homogeneous. This is an interesting observation as the increased toxicity of such molecules could be compensated by their limited membrane-destructive activity. In our studies based on Langmuir monolayers, two models of fungal plasma membrane were investigated: M1 of the same composition as that applied for GUV formation and M2 in which the main component POPC was exchanged to the saturated-chain DPPC. As it was proved by BAM, in contrast to M1, the M2 model is not homogenous but condensed 2D crystalline domains form in this monolayer being in equilibrium with

less organized LE regions. Thus, this model can simulate the formation of lipid rafts in the fungal membrane.

The amount of PAH molecules which could be incorporated into the model fungal membrane depends significantly both on the membrane composition and on the structure of the PAH molecule. BAP was most efficiently incorporated in the more expanded M1 model of the membrane, whereas the incorporation of the isomeric PAHs fluoranthene and pyrene as well as their nitro derivatives was mutually comparable, and limited compared with BAP. These trends were partially reversed at the application of the more condensed M2 model. There, FLU and NFLU were most efficiently incorporated into the membrane. However, Brewster angle microscopy and GIXD experiments proved that, depending on its structure, the PAH molecule can be distributed between the liquid expanded and liquid condensed domains of the monolayer. FLU and NFLU preferred the LE regions of the monolayer, whereas PYR, BAP and their nitro derivatives could be incorporated into the 2D crystalline domains affecting the packing of the film-forming molecules. This is an important observation as it indicates that PAHs and nitro-PAHs can affect the organization of lipid rafts in the fungal plasma membrane.

Summing up, our results prove that nitro-PAHs, which were reported to be highly toxic to bacteria [45], are less destructive to model fungal membranes than the native unsubstituted PAH counterparts. This holds promise for the application of non-ligninolytic fungi in bioremediation. Hopefully, future *in-vitro* studies will support these results, helping in the search of fungal species applicable in bioaugmentation.

Author statement

Aneta Wójcik – was a PhD student of Marcin Broniatowski. She was responsible for the GUV measurements and Langmuir experiments, elaborated the data, prepared the draft version of the article.

Mareike Stefan – collaborated with Aneta Wójcik at her stay in Potsdam at the experiments regarding GUVs and DSC experiments, collaborated with AW at the the data curation and elaboration, reviewed the draft of the manuscript.

Weronika Ryczek – was the MSc student of Marcin Broniatowski. Measured the π-A isotherms and BAM images, elaborated the data.

Karolina Olechowska – performed part of the Langmuir and BAM experiments, prepared a part of the manuscript, reviewed the draft of the manuscript.

Paweł Wydro – Together with MB performed the GIXD experiments, elaborated the GIXD data, prepared a part of the manuscript, reviewed the draft of the manuscript.

Rumiana Dimova – Supervised AW and MS in Potsdam. Took part in the conceptualization of the measurements devoted to GUVs, supervised the data elaboration, reviewed the draft of the manuscript.

Marcin Broniatowski – was responsible for the general conceptualization of the project, supervised it at all stages, together with PW performed the GIXD experiments and elaborated the data, supervised the preparation of the draft of the manuscript, its corrections and its final form.

Declaration of Competing Interest

The authors declare that they have no known competing financial interests or personal relationships that could have appeared to influence the work reported in this paper.

Acknowledgement

This project was financed by the National Science Centre (No 2016/ 21/B/ST5/00245). We gratefully acknowledge SOLEIL for provision of synchrotron radiation facilities and we would like to thank Dr. Philippe Fontaine for assistance in using SIRIUS beamline.

References

[1] A.B. Patel, S. Shaikh, K.R. Jain, C. Desai, D. Madamwar, Polycyclic aromatic hydrocarbons: Sources, toxicity, and remediation approaches, Front. Microbiol. 11 (2020) 562813.
[2] F. Wania, D. Mackay, Tracking the distribution of persistent organic pollutants, Environ. Sci. Technol. 30 (1996) 390–396.
[3] A. Ball, A. Truskewycz, Polyaromatic hydrocarbon exposure: an ecological impact ambiguity, Environ Sci Pollut Res 20 (7) (2013) 4311–4326.
[4] O. Idowu, K.T. Semple, K. Ramadass, W. O'Connor, P. Hansbro, P. Thavamani, Beyond the obvious: Environmental health implications of polar polycyclic aromatic hydrocarbons, Environ. Internat. 123 (2019) 543–557.
[5] M. Honda, N. Suzuki, Toxicities of polycyclic aromatic hydrocarbons for aquatic animals, Int. J. Environ. Res. Public Health 17 (2020) 1363.
[6] B. Ewa, M.-Š. Danuta, Polycyclic aromatic hydrocarbons and PAH-related DNA adducts, J. Appl. Genetics 58 (3) (2017) 321–330.
[7] E. Reizer, B. Viskolcz, B. Fiser, Formation and growth mechanism of polycyclic aromatic hydrocarbons: A mini-review, Chemosphere 291 (2022) 132793.
[8] N. Kiprotich Cheruiyot, W.J. Lee, J. Kennedy Mwangi, L.C. Wang, N.H. Lin, Y.C. Lin, J. Cao, R. Zhang, G.P. Chang-Chien, An overview: Polycyclic aromatic hydrocarbon emissions from the stationary and mobile sources and in the ambient air, Aerosol Air Qual, Res. 15 (2015) 2730–2762.
[9] K. Ravindra, R. Sokhia, R. Van Grieken, Atmospheric polycyclic aromatic hydrocarbons: Source attribution, emission factors and regulation, Atmosph. Environ. 42 (2008) 2895–2921.
[10] H. Hua, M. Tian, L. Zhang, F. Yang, C. Peng, Y. Chen, G. Shi, X. Yao, C. Jiang, J. Wang, Sources and gas-particle partitioning of atmospheric parent, oxygenated, and nitrated polycyclic aromatic hydrocarbons in a humid city in southwest China, Atmosph. Environ. 206 (2019) 1-10.
[11] A. Krzyszczak, B. Czech, Occurrence and toxicity of polycyclic aromatic hydrocarbons derivatives in environmental matrices, Sci. Total. Environ. 788 (2021) 147738.
[12] A. Ramesh, S.A. Walker, D.B. Hood, M.D. Guillén, K. Schneider, E.H. Weyand, Bioavailability and risk assessment of orally ingested polycyclic aromatic hydrocarbons, Int. J. Toxicol. 23 (5) (2004) 301–333.
[13] I. Zwirner-Baier, H.-G. Neumann, Polycyclic nitroarenes (nitro-PAHs) as biomarkers of exposure to diesel exhaust, Mutation Res. 441 (1) (1999) 135–144.
[14] M. Watanabe, Y. Noma, Influence of combustion temperature on formation of nitro-PAHs and decomposition and removal behaviors in pilot-scale waste incinerator, Environ. Sci. Technol. 43 (7) (2009) 2512–2518.
[15] F. Reisen, J. Arey, Atmospheric reactions influence seasonal PAH and nitro-PAH concentrations in the Los Angeles basin, Environ. Sci. Technol. 39 (1) (2005) 64–73.
[16] J. Yan, X. Wang, P. Gong, C. Wang, Nitrated polycyclic aromatic compounds in the atmospheric environment: A review, Crit. Rev. Environ. Sci. Technol. 51 (11) (2021) 1159–1185.
[17] R. Atkinson, J. Arey, Atmospheric chemistry of gas-phase polycyclic aromatic hydrocarbons: Formation of atmospheric mutagens, Environ. Health Persp. 102 (Suppl. 4) (1994) 117–124.
[18] B.A. Musa Bandowe, H. Meusel, Nitrated polycyclic aromatic hydrocarbons (nitro-PAHs) in the environment – A review, Sci. Total Environ. 581–582 (2017) 237–257.
[19] J.L. Durant, W.F. Busby, A.L. Lafleur, B.W. Penman, C.L. Crespi, Human cell mutagenicity of oxygenated, nitrated and unsubstituted polycyclic aromatic hydrocarbons associated with urban aerosols, Mutation Res. 371 (3-4) (1996) 123–157.
[20] I.J. Keyte, R.M. Harrisonz, G. Lammelbc, Chemical reactivity and long-range transport potential of polycyclic aromatic hydrocarbons – a review, Chem. Soc. Rev. 42 (2013) 9333–9391.
[21] J. de Boer, M. Wagelmans, Polycyclic aromatic hydrocarbons in soil – Practical options for remediation, Clean – Soil, Air, Water 44 (2016) 648–653.
[22] P.P. Falciglia, G. De Guidi, A. Catalfo, F.G.A. Vagliasindi, Remediation of soils contaminated with PAHs and nitro-PAHs using microwave irradiation, Chem. Eng. J. 296 (2016) 162–172.
[23] G. Gbeddy, A. Goonetilleke, G.A. Ayoko, P. Egodawatta, Transformation and degradation of polycyclic aromatic hydrocarbons (PAHs) in urban road surfaces: Influential factors, implications and recommendations, Environ. Pollut. 257 (2020) 113510.
[24] D. Zhang, D. Zhi, W. Chen, Sorption of nitroaromatics to soils: Comparison of the importance of soil organic matter versus clay, Environ. Toxicol. Chem. 28 (2009) 1447–1454.
[25] D. Ghosal, S. Ghosh, T.K. Dutta, Y. Ahn, Current state of knowledge in microbial degradation of polycyclic aromatic hydrocarbons (PAHs): A review, Front. Microbiol. 7 (2016) 1369.
[26] X. Ren, G. Zeng, L. Tang, J. Wang, J. Wan, Y. Liu, J. Yu, H. Yi, S. Ye, R. Deng, Sorption, transport and biodegradation – An insight into bioavailability of persistent organic pollutants in soil, Sci. Total Environ. 610–611 (2018) 1154–1163.

[27] A. Cachada, R. Pereira, E. Ferreira da Silva, A.C. Duarte, The prediction of PAHs bioavailability in soils using chemical methods: State of the art and future challenges, Sci. Total Environ. 472 (2014) 463–480.
[28] B. Wei, C. Liu, J. Bao, Y. Wang, J. Hu, M. Qi, J. Jin, Y. Wei, Uptake and distributions of polycyclic aromatic hydrocarbons in cultivated plants around an E-waste disposal site in Southern China, Environ. Sci. Pollut. Res. 28 (3) (2021) 2696–2706.
[29] R.A. Kanaly, S. Harayama, Advances in the field of high-molecular-weight polycyclic aromatic hydrocarbon biodegradation by bacteria, Microb. Biotechnol. 3 (2) (2010) 136–164.
[30] E. Doyle, L. Muckian, A.M. Hickey, N. Clipson, Microbial PAH degradation, Adv. Appl. Microbiol. 65 (2008) 27–66.
[31] A.K. Haritash, C.P. Kaushik, Biodegradation aspects of polycyclic aromatic hydrocarbons (PAHs): A review, J. Hazard. Mater. 169 (1-3) (2009) 1–15.
[32] M.C. Cecilia, M. Guivernau, X. Moreno-Ventas, F.X. Prenafeta-Boldú, M. Viñas, Bioaugmentation of native fungi, an efficient strategy for the bioremediation of an aged industrially polluted soil with heavy hydrocarbons, Front. Microbiol. 12 (2021) 626436.
[33] E.O. Atakpa, H. Zhou, L. Jiang, Y. Ma, Y. Liang, Y. Li, D. Zhang, C. Zhang, Improved degradation of petroleum hydrocarbons by co-culture of fungi and biosurfactant-producing bacteria, Chemosphere 290 (2022) 133337.
[34] H. Harms, D. Schlosser, L.Y. Wick, Untapped potential: exploiting fungi in bioremediation of hazardous chemicals, Nature, Rev. Microbiol. 9 (2011) 177–192.
[35] S. Furuno, K. Päzolt, C. Rabe, T.R. Neu, H. Harms, L.Y. Wick, Fungal mycelia allow chemotactic dispersal of polycyclic aromatic hydrocarbon-degrading bacteria in water-unsaturated systems, Environ. Microbiol. 12 (2010) 1391–1398.
[36] A. Imam, S. Kumar Suman, P.K. Kanaujia, A. Ray, Biological machinery for polycyclic aromatic hydrocarbons degradation: A review, Biores. Technol. 343 (2022) 126121.
[37] N. Agrawal, A. Barapatre, M.P. Shahi, S.K. Shahi, Biodegradation pathway of polycyclic aromatic hydrocarbons by ligninolytic fungus Podoscypha elegans strain FTG4 and phytotoxicity evaluation of their metabolites, Environ. Process. 8 (3) (2021) 1307–1335.
[38] G. Gramss, K.D. Voigt, B. Kirsche, Degradation of polycyclic aromatic hydrocarbons with three to seven aromatic rings by higher fungi in sterile and unsterile soils, Biodeg. 10 (1999) 51–62.
[39] A. Arun, M. Eyini, Comparative studies on lignin and polycyclic aromatic hydrocarbons degradation by basidiomycetes fungi, Bioresource Technol. 102 (17) (2011) 8063–8070.
[40] A. Reyes-César, Á.E. Absalón, F.J. Fernández, J.M. González, D.V. Cortés-Espinosa, Biodegradation of a mixture of PAHs by non-ligninolytic fungal strains isolated from crude oil-contaminated soil, World J. Microbiol. Biotechnol. 30 (3) (2014) 999–1009.
[41] E. Marco-Urrea, I. García-Romera, E. Aranda, Potential of non-ligninolytic fungi in bioremediation of chlorinated and polycyclic aromatic hydrocarbons, New Biotechnol. 32 (6) (2015) 620–628.
[42] A. Verdin, A. Lounès-Hadj Sahraoui, R. Newsam, G. Robinson, R. Durand, Polycyclic aromatic hydrocarbons storage by Fusarium solani in intracellular lipid vesicles, Environ. Pollut. 133 (2) (2005) 283–291.
[43] G. Zafra, A.E. Absalón, D.V. Cortés-Espinosa, Morphological changes and growth of filamentous fungi in the presence of high concentrations of PAHs, Braz. J. Microbiol. 46 (2015) 937–941.
[44] J. Sikkema, J.A.M. de Bont, B. Poolman, Mechanism of membrane toxicity of hydrocarbons, Microbiol. Rev. 59 (1995) 201–222.
[45] R.L. Crawford, The microbiology and treatment of nitroaromatic compounds, Curr. Opin. Biotechnol. 6 (1995) 329–336.
[46] J.C. Spain, Biodegradation of nitroaromatic compounds, Annu. Rev. Microbiol. 49 (1) (1995) 523–555.
[47] A. Esteve-Núñez, A. Caballero, J.L. Ramos, Biological degradation of 2,4,6-trinitrotoluene, Microbiol. Molec, Biol. Rev. 65 (3) (2001) 335–352.
[48] J.D. Stahl, S.D. Aust, Plasma membrane dependent reduction of 2,4,6-trinitrotoluene by *Phanerchaete chrysosporium*, Biochem. Biophys. Res. Commun. 192 (1993) 471–476.
[49] S. Li, Y. Huang, M. Zhang, Y. Gao, C. Pan, K. Deng, B. Fan, Remediation of 1-nitropyrene in soil: A comparative study with pyrene, Int. J. Environ. Res. Public Health 17 (2020) 1914.
[50] T. Ramdahl, B. Zielinska, J. Arey, R. Atkinson, A.M. Winer, J.N. Pitts, Ubiquitous occurrence of 2-nitrofluoranthene and 2-nitropyrene in air, Nature 321 (6068) (1986) 425–427.
[51] M. Cazaunau, K. Le Ménach, H. Budzinski, E. Villenave, Atmospheric heterogeneous reactions of benzo(a)pyrene, Z. Phys. Chem. 224 (2010) 1151–1170.
[52] R. Dimova, C. Marques, The Giant Vesicle Book, Taylor & Francis Group, LLC, Boca Raton, FL, USA, 2019.
[53] R. Dimova, Annu. Rev. Biophys. 48 (2019) 93.
[54] A. Weinberger, F.-C. Tsai, G. Koenderink, T. Schmidt, R. Itri, W. Meier, T. Schmatko, A. Schröder, C. Marques, Gel-assisted formation of giant unilamellar vesicles, Biophys. J. 105 (1) (2013) 154–164.
[55] J.T. Davies, E.K. Rideal, Interfacial Phenomena, Academic Press, New York, 1961.
[56] P. Fontaine, G. Ciatto, N. Aubert, M. Goldmann, Soft interfaces and resonant investigation on undulation source: A surface X-ray scattering beamline to study organic molecular films at the SOLEIL synchrotron Sci, Adv. Mater. 6 (2014) 2312–2316.
[57] K. Kjaer, Some simple ideas on X-ray reflection and grazing-incidence diffraction from thin surfactant films, Physica B 198 (1-3) (1994) 100–109.
[58] J. Als-Nielsen, D. Jacquemain, K. Kjaer, F. Leveiller, M. Lahav, L. Leiserowitz, Principles and applications of grazing incidence X-ray and neutron scattering from ordered molecular monolayers at the air-water interface, Phys. Rep. 246 (5) (1994) 251–313.
[59] P.J. Brennan, D.M. Losel, Physiology of fungal lipids: Selected topics, Adv. Microb. Physiol. 17 (1978) 47–179.
[60] C. Klose, M.A. Surma, M.J. Gerl, F. Meyenhofer, A. Shevchenko, K. Simons, M. Polymenis, Flexibility of a eukaryotic lipidome – Insights from yeast lipidomics, PLoS ONE 7 (4) (2012) e35063.
[61] E. Zinser, C.D. Sperka-Gottlieb, E.V. Fasch, S.D. Kohlwein, F. Paltauf, G. Daum, Phospholipid synthesis and lipid composition of subcellular membranes in the unicellular eukaryote *Saccharomyces* cerevisiae, J. Bacteriol. 173 (6) (1991) 2026–2034.
[62] A.I.P.M. de Kroon, P.J. Rijken, C.H. De Smet, Checks and balances in membrane phospholipid class and acyl chain homeostasis, the yeast perspective, Prog. Lipid Res. 52 (4) (2013) 374–394.
[63] Y. Zhu, L.u. Wu, J. Zhu, Y. Xu, Q. Yong, S. Yu, Quantitative lipidomic insights in the inhibitory response of Pichia stipitis to vanillin, 5-hydroxymethylfurfural, and acetic acid, Biochem. Biophys. Res. Commun. 497 (1) (2018) 7–12.
[64] 8. P. Stolarek, S. Różalska, P. Bernat, Lipidomic adaptations of the *Metarhizium robertsii* strain in response to the presence of butyltin compounds, Biochim. Biophys. Acta 1861 (2019) 316–326.
[65] M.F. Renne, A.I.P.M. de Kroon, The role of phospholipid molecular species in determining the physical properties of yeast membranes, FEBS Lett. 592 (8) (2018) 1330–1345.
[66] S. Wagner, F. Patauf, Generation of glycerophospholipid molecular species in the yeast *Saccharomvces cerevisiae*. Fatty acid pattern of phospholipid classes and selective acyl turnover at sn-1 and *sn-2* positions, Yeast 10 (1994) 1429–1437.
[67] F.L. Linhares de Aguiar, N.C. Santos, C.S. de Paula Cavalcante, D. Andreu, G.R. Baptista, S. Gonçalves, Antibiofilm activity on Candida albicans and mechanism of action on biomembrane models of the antimicrobial peptide Ctn[15–34], Int. J. Molec. Sci. 21 (2020) 8339.
[68] F. Foglia, M.J. Lawrence, B. Deme, G. Fragneto, D. Barlow, Neutron diffraction studies of the interaction between amphotericin B and lipid-sterol model membranes, Sci. Rep. 2 (2012) 778.
[69] M.E. van der Rest, A.H. Kamminga, A. Nakano, Y. Anraku, B. Poolman, W.N. Konings, The plasma membranes of *Saccharomyces cerevisiae*. Structure, function and biogenesis, Microbiol. Rev. 59 (1995) 304–322.
[70] L.M. Douglas, J.B. Konopka, Fungal membrane organization: The eisosome concept, Annu. Rev. Microbiol. 68 (1) (2014) 377–393.
[71] Z.e. Chen, Z. Zheng, C. Yi, F. Wang, Y. Niu, H. Li, Intracellular metabolic changes in Saccharomyces cerevisiae and promotion of ethanol tolerance during the bioethanol fermentation process, RSC Adv. 6 (107) (2016) 105046–105055.
[72] T.T. Bui, K. Suga, H. Umakoshi, Roles of sterol derivatives in regulating the properties of phospholipid bilayer systems, Langmuir 32 (2016) 6176–6184.
[73] A. Felczak, P. Bernat, S. Różalska, K. Lisowska, Quinoline biodegradation by filamentous fungus Cunninghamella elegans and adaptive modifications of the fungal membrane composition, Environ. Sci. Pollut. Res. 23 (9) (2016) 8872–8880.
[74] D.A. Wilkinson, J.F. Nagle, Metastability in the phase behavior of dimyristoylphosphatidylethanolamine bilayers, Biochem. 23 (7) (1984) 1538–1541.
[75] P. Bernat, J. Nykiel-Szymańska, P. Stolarek, M. Słaba, R. Szewczyk, S. Różalska, 2,4-dichlorophenoxyacetic acid-induced oxidative stress: Metabolome and membranę modifications in *Umbelopsis isabellina*, a herbicide degrader, PlOS ONE 13 (2018) e0199677.
[76] Y. Barenholz, T. Cohen, R. Korenstein, M. Ottolenghit, Organization and dynamics of pyrene and pyrene lipids in intact lipid bilayers, Biophys. J. 59 (1991) 110–124.
[77] J. Huang, Y. Wu, Y. Chen, Z. Zhu, X. Yang, C.J. Yang, K. Wang, W. Tan, Pyrene-excimer probes based on the hybridization chain reaction for the detection of nucleic acids in complex biological fluids, Angew. Chem. Int. Ed. 50 (2) (2011) 401–404.
[78] S.A. Bortolato, J.A. Arancibia, G.M. Escandar, A novel application of nylon membranes to the luminescent determination of benzo[a]pyrene at ultra trace levels in water samples, Anal. Chim. Acta 613 (2) (2008) 218–227.
[79] C. Stefaniu, G. Brezesinski, H. Möhwald, Langmuir monolayers as models to study processes at membrane surfaces, Adv. Colloid Interface Sci. 208 (2014) 197–213.
[80] M. Maaloum, P. Muller, M.P. Krafft, Lateral and vertical nanophase separation in Langmuir-Blodgett films of phospholipids and semifluorinated alkanes, Langmuir 20 (6) (2004) 2261–2264.
[81] M. Broniatowski, M. Binczycka, A. Wójcik, M. Flasiński, P. Wydro, Polycyclic aromatic hydrocarbons in model bacterial membranes – Langmuir monolayer studies, Biochim. Biophys. Acta 1859 (12) (2017) 2402–2412.
[82] B. Korchowiec, Y. Corvis, T. Viitala, C. Feidt, Y. Guiavarch, C. Corbier, E. Rogalska, Interfacial approach to polyaromatic hydrocarbon toxicity: Phosphoglyceride and cholesterol monolayer response to phenantrene, anthracene, pyrene, chrysene, and benzo[a]pyrene, J. Phys. Chem. B 112 (2008) 13518–13531.
[83] M. Słaba, P. Bernat, S. Rożalska, J. Nykiel, J. Długoński, Comparative study of metal induced phospholipid modifications in the heavy metal tolerant

filamentous fungus *Paecilomyces marquandii* and implications for the fungal membrane integrity, Acta Biochim. Pol. 60 (2013) 695–700.
[84] K. Hąc-Wydro, M. Flasiński, M. Broniatowski, M. Sołtys, Studies on the behavior of eucalyptol and terpinen-4-ol – natural food additives and ecological pesticides – in model lipid membranes, Langmuir 33 (27) (2017) 6916–6924.
[85] P. Perczyk, A. Wójcik, P. Wydro, M. Broniatowski, The role of phospholipid composition and ergosterol presence in the adaptation of fungal membranes to harsh environmental conditions–membrane modeling study, Biochim. Biophys. Acta 1862 (2020).
[86] L. Wiegart, B. Struth, Geometric boundary condition for the chain alignment in lipid monolayers, Physica B 357 (1-2) (2005) 126–129.
[87] J. Liu, J. Jia, P. Grathwohl, Dilution of concentrations of PAHs from atmospheric particles, bulk deposition to soil: a review, Environ. Geochem. Health, doi.org/10.1007/s10653-022-01216-w.
[88] S.S. Bhattacharya, K. Syed, J. Shann, J.S. Yadav, A novel P450-initiated biphasic process for sustainable biodegradation of benzo[a]pyrene in soil under nutrient-sufficient conditions by the white rot fungus *Phanerochaete chrysosporium*, J. Hazard. Mater. 261 (2013) 675–683.
[89] F. Acevedo, L. Pizzul, M.D.P. Castillo, R. Cuevas, M.C. Diez, Degradation of polycyclic aromatic hydrocarbons by the Chilean white-rot fungus *Anthracophyllum discolor*, J. Hazard. Mater. 185 (1) (2011) 212–219.
[90] Y.W. Hsueh, K. Gilbert, C. Trandum, M. Zuckermann, J. Thewalt, The effect of ergosterol on dipalmitoylphosphatidylcholine bilayers: A deuterium NMR and calorimetric study, Biophys. J. 88 (2005) 1799–1808.
[91] R. Lipowsky, R. Dimova, Domains in membranes and vesicles, J. Phys. Condens. Matter 15 (1) (2003) S31–S45.